Heliyon 10 (2024) e35062

Contents lists available at ScienceDirect

Heliyon

journal homepage: www.cell.com/heliyon

Research article

# A new strategy for immobilization of copper on the $Fe_3O_4$@EDTA nanocomposite and its efficient catalytic applications in reduction and one-pot reductive acetylation of nitroarenes and also *N*-acetylation of arylamines

Leila Mavaddatiyan, Behzad Zeynizadeh *

*Department of Organic Chemistry, Faculty of Chemistry, Urmia University, Urmia, Iran*

ARTICLE INFO

*Keywords:*
Copper
EDTA
$Fe_3O_4$
Nitroarene
Reduction
Reductive acetylation

ABSTRACT

A new and efficient Cu(II)-containing mesoporous nanocatalytic system was synthesized by direct immobilization of copper metal powder on the $Fe_3O_4$@EDTA nanocomposite. The as-prepared $Fe_3O_4$@EDTA@Cu(II) nanocomposite was then characterized by FT-IR, XRD, SEM, TEM, SEM-based EDX and elemental mapping, XPS, TGA, VSM, and also BET and BJH analyses. The resulting $Fe_3O_4$@EDTA@Cu(II) mesoporous nanocomposite exhibited satisfactory catalytic activity towards the reduction and one-pot reductive acetylation of nitroarenes and also N-acetylation of arylamines in water at 60 °C. Notably, the applied Cu(II)-containing nanocatalyst was efficiently recovered from the reaction mixture using an external magnetic field and could be reused successfully for five cycles. The protocol developed in this study offers several advantages in terms of mild reaction conditions, simple workflows, using water as a green solvent, and easy recovery and catalyst reuse, making it more ecologically and economically attractive.

## 1. Introduction

Green chemistry aims to develop sustainable and efficient chemical synthesis methods and production while minimizing environmental impact [1–7]. One of the noteworthy aspects of green chemistry is using eco-friendly solvents for chemical reactions. In this regard, water is used widely as a green solvent for chemical reactions due to its abundance, low cost, and non-toxicity [8–15]. Another aim of green chemistry is to remove toxic substances that are dangerous for the ecosystems. One of these substances is nitrobenzene ($PhNO_2$) and some of its derivatives, which have various harmful effects on humans, animals, and the environment [16–20]. Reduction of the hazardous nitrobenzene and its derivatives with nanocatalysts is widely evaluated and used in academic laboratories and the chemical industry. Notably, the mentioned reduction reaction of aromatic nitro compounds is a crucial process in the chemical industry, with various applications in the production of different chemicals and materials such as surfactants, emulsifiers, nylon, pesticides, herbicides, and pharmaceuticals [21–25]. Furthermore, when aniline ($PhNH_2$), as a product of the $PhNO_2$ reduction, undergoes acetylation, lead produces *N*-arylacetamides, which is an essential intermediate in organic synthesis for the production of various drugs, including acetaminophen (paracetamol), lidocaine, mepivacaine, prilocaine, chloroquine, sulfonamides, and many other drug-like compounds [26–33].

* Corresponding author.
*E-mail address:* bzeynizadeh@gmail.com (B. Zeynizadeh).

https://doi.org/10.1016/j.heliyon.2024.e35062
Received 27 April 2024; Received in revised form 21 July 2024; Accepted 22 July 2024
Available online 26 July 2024

In recent years, there has been increasing interest in developing new and durable nanocatalysts, especially magnetically recoverable and reusable ones, with simple structures and incorporating inexpensive metals that can still maintain high performance and selectivity in organic synthesis because conventional catalytic systems can be expensive to produce and often require complex synthesis methods, which can limit their widespread use in industry [34–38]. To make a new recyclable catalyst, in addition to a magnetic core (such as $Fe_3O_4$, $CuFe_2O_4$, $MnFe_2O_4$, etc.), we need a suitable substrate to hold the metal components in the final structure of the catalyst. In this regard, ethylenediaminetetraacetic acid (EDTA), known as an ordinary and powerful organic chelating agent, can form extremely stable, highly soluble, and hardly biodegradable chelates with most metallic elements, including copper (Cu), nickel (Ni), chromium (Cr), and ferrite (Fe) [39]. On the other hand, choosing and using the proper and effective metal in the last layer of the catalyst is essential. Copper (Cu) is a 3d earth-abundant transition metal (EATM) whose materials have been widely used in numerous catalytic organic reactions due to its various oxidation states from zero to positive 3 [40–44].

In continuation of our research program upon designing efficient catalytic systems for various organic transformations [45–51] and also, due to the reputation of introducing new green protocols to the conversion of nitroarenes to valuable organic compounds, herein we wish to report a new strategy for immobilization of copper(II) using pure copper metal powder on the $Fe_3O_4$@EDTA nanocomposite and investigation of the as-prepared $Fe_3O_4$@EDTA@Cu(II) catalytic applications in the green reduction and one-pot reductive acetylation of nitroarenes and also *N*-acetylation of arylamines in water.

## 2. Results and discussion

### 2.1. Preparation and characterization of the $Fe_3O_4$@EDTA@Cu(II) nanocomposite

The process for creating the $Fe_3O_4$@EDTA@Cu(II) nanocomposite is illustrated in Fig. 1. First of all, the $Fe_3O_4$ nanoparticles (NPs) are synthesized using the co-precipitation method. In the next step, the surface of the $Fe_3O_4$ NPs is modified with EDTA. Eventually, the Cu(II) NPs are immobilized on the modified EDTA using pure copper metal, resulting in the desired $Fe_3O_4$@EDTA@Cu(II) nanocomposite. After the $Fe_3O_4$@EDTA@Cu(II) nanocomposite preparation, we characterized the structure of mentioned nanocomposite by Fourier transform infrared spectroscopy (FT-IR), X-ray diffraction (XRD), scanning electron microscopy (SEM), transmission electron microscopy (TEM), SEM-based energy dispersive X-ray (EDX) and elemental mapping, X-ray photoelectron spectroscopy (XPS), thermogravimetric analysis (TGA), vibrating sample magnetometer (VSM), and Brunauer–Emmett–Teller (BET) and Barrett–Joyner–Halenda (BJH) analyses.

The FT-IR spectroscopy of the $Fe_3O_4$, $Fe_3O_4$@EDTA, and $Fe_3O_4$@EDTA@Cu(II) nanostructures was carried out using the potassium bromide (KBr) disk method, and all of the spectra were recorded in the region 400–4000 $cm^{-1}$, as shown in Fig. 2. In the FT-IR spectra of the $Fe_3O_4$@EDTA@Cu(II) nanocomposite, the broad peak at 3429 $cm^{-1}$ is related to the OH stretching vibrations. Also, the peaks at 2935 $cm^{-1}$, 2923 $cm^{-1}$, and 2850 $cm^{-1}$ are related to the C–H stretching vibrations. Furthermore, the peak at 1618 $cm^{-1}$ corresponds to the C=O stretching vibrations, whereas the peaks at 1384 $cm^{-1}$, 1216 $cm^{-1}$, and 1157 $cm^{-1}$ can be related to the C–O–H (bending), C–O (stretching), and C–N (stretching), respectively. Notably, the peaks at 630 $cm^{-1}$ and 580 $cm^{-1}$ related to the splitting $\nu_1$ vibration mode of $Fe^{2+}$—$O^{2-}$ and $Cu^{2+}$—$O^{2-}$, whereas the peak at 430 $cm^{-1}$ corresponds to the splitting $\nu_2$ vibration mode of $Fe^{3+}$—$O^{2-}$.

The X-ray diffraction (XRD) spectra of the $Fe_3O_4$, $Fe_3O_4$@EDTA, and $Fe_3O_4$@EDTA@Cu(II) nanostructures are recorded in a range of Bragg's angle ($2\theta = 10$–$80°$) at room temperature (Fig. 3). The XRD pattern of the prepared $Fe_3O_4$ NPs reveals nine characteristic peaks at $2\theta = 18.34°$, 30.28°, 35.54°, 43.31°, 53.62°, 57.25°, 62.85°, 71.28°, and 74.21°, which matched well with Joint Committee on

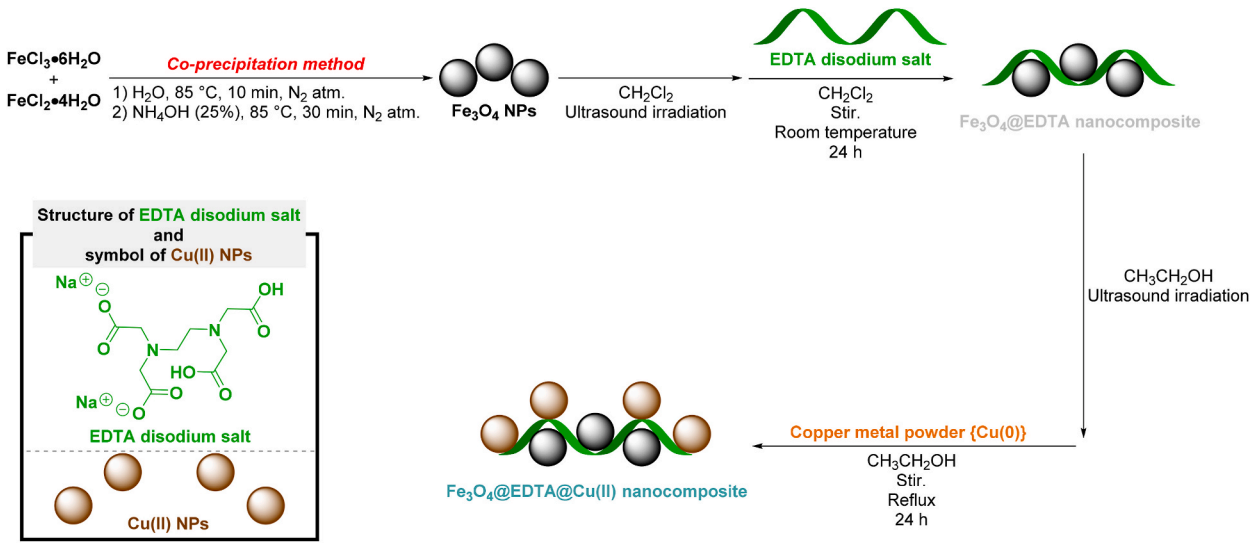


**Fig. 1.** Preparation of the $Fe_3O_4$@EDTA@Cu(II) nanocomposite.

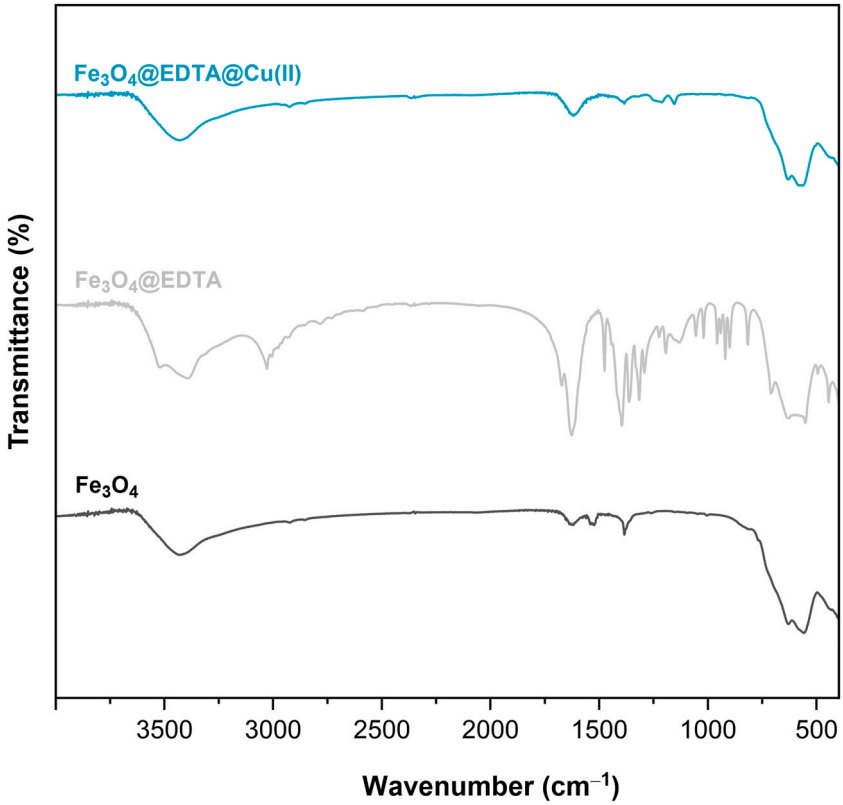


**Fig. 2.** FT-IR diagrams of the $Fe_3O_4$, $Fe_3O_4$@EDTA, and $Fe_3O_4$@EDTA@Cu(II) nanostructures.

Powder Diffraction Standards (JCPDS) cards, file no. 79–0418, 65–3107, 74–2402, 01-075-0449, and 98-007-7842. Comparison of the obtained pattern for $Fe_3O_4$@EDTA@Cu(II) nanocomposite with the XRD peaks of $Fe_3O_4$ composition indicates that the relative position and intensity of all peaks correspond to the standard pattern, suggesting that the spinel crystal structure is preserved during the functionalization process.

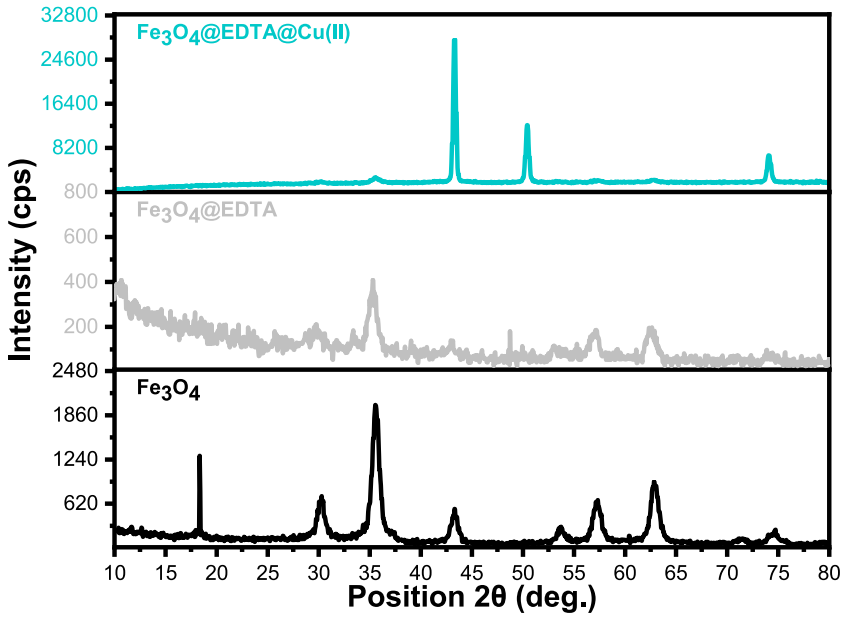


**Fig. 3.** XRD diagrams of the $Fe_3O_4$, $Fe_3O_4$@EDTA, and $Fe_3O_4$@EDTA@Cu(II) nanostructures.

The SEM (Fig. 4) and TEM (Fig. 5) images provide insights into the particle size and morphology of the as-prepared $Fe_3O_4$@EDTA@Cu(II) nanocomposite. The mentioned images indicate that $Fe_3O_4$@EDTA@Cu(II) exhibits a predominantly monodisperse distribution and has a rough surface texture. Also, based on SEM images (Fig. 4), the particle size range of the $Fe_3O_4$@EDTA@Cu(II) nanocomposite is from 22 to 100 nm. On the other hand, the SEM-based energy-dispersive X-ray (EDX) (Fig. 6) and elemental mapping (Fig. 7) analyses were conducted to validate the $Fe_3O_4$@EDTA@Cu(II) composition elements. In this regard, the EDX analysis (Fig. 6) provided the percentage of the elements, including 32.7 w%, 29.8 w%, 28.3 w%, 6.3 w%, and 3.0 w% for C, Fe, O, N, and Cu, respectively.

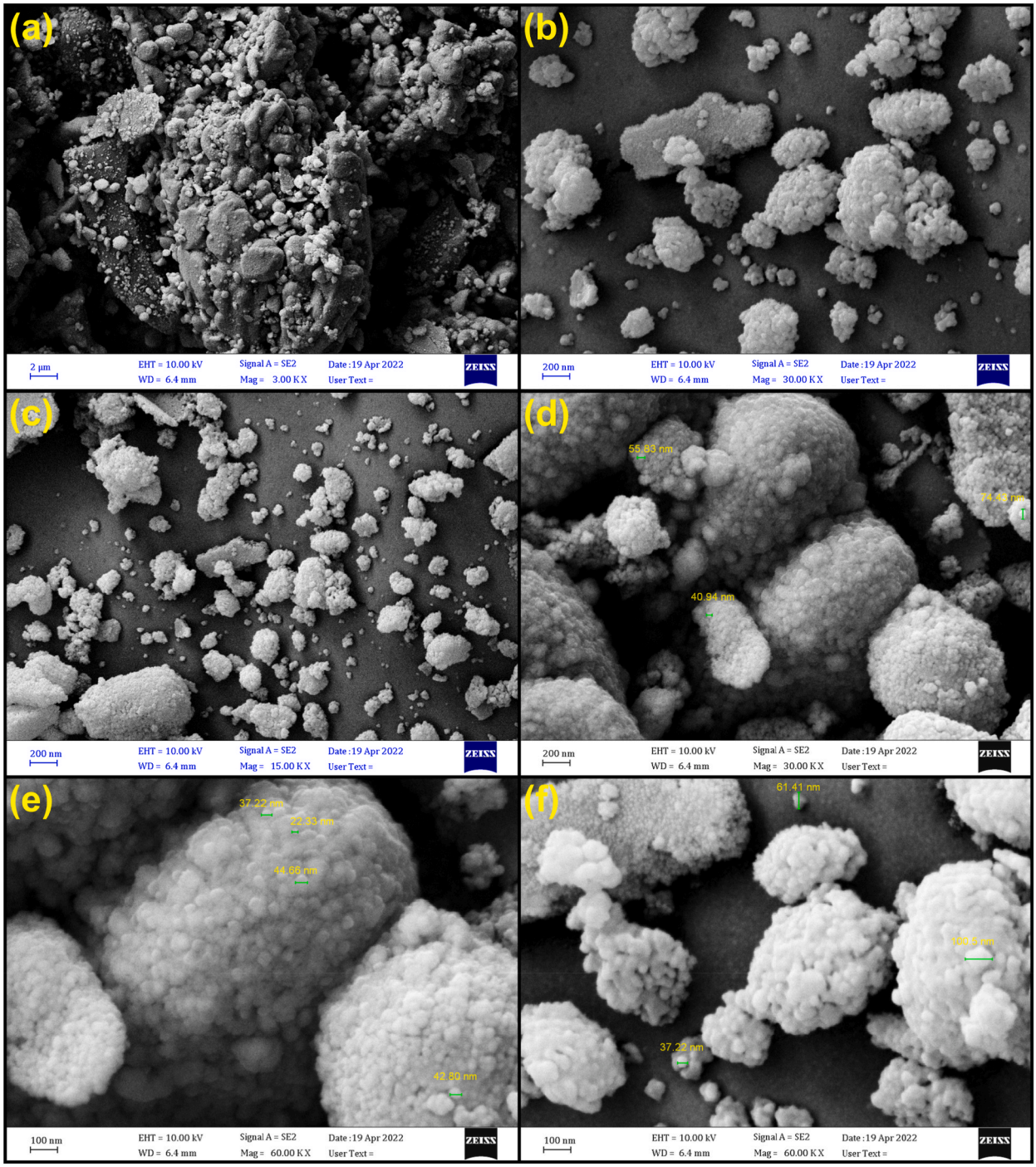


**Fig. 4.** SEM images of the as-prepared $Fe_3O_4$@EDTA@Cu(II) nanocomposite.

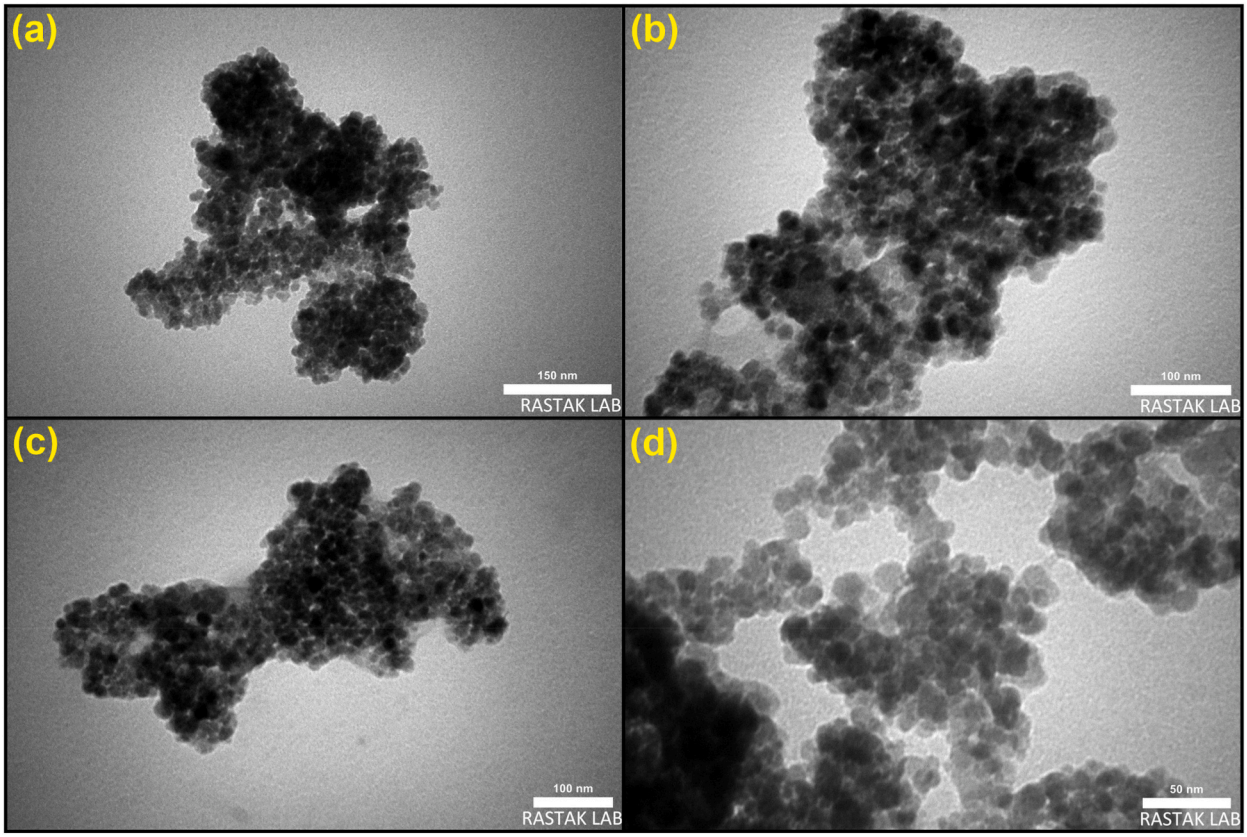


**Fig. 5.** TEM images of the as-prepared $Fe_3O_4$@EDTA@Cu(II) nanocomposite.

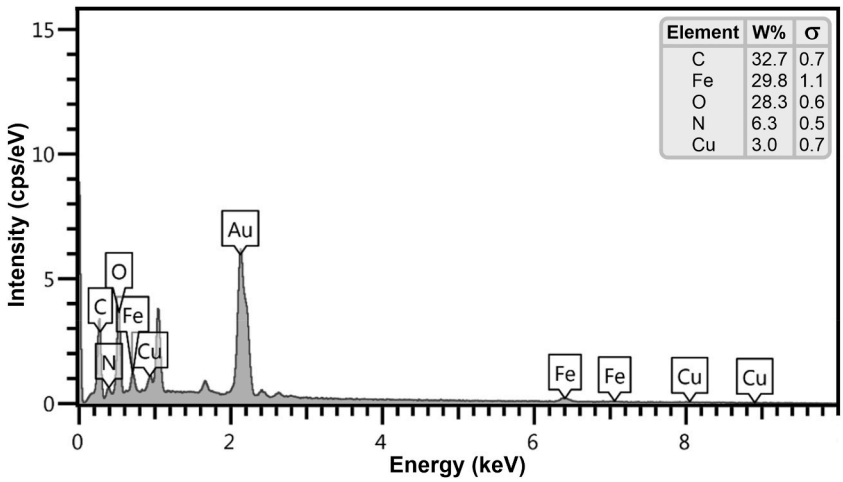


**Fig. 6.** SEM-based EDX diagram of the $Fe_3O_4$@EDTA@Cu(II) nanocomposite.

The elemental chemical composition and chemical valence state of the as-prepared $Fe_3O_4$@EDTA@Cu(II) nanocomposite were investigated by X-ray photoelectron spectroscopy (XPS). The related XPS total spectrum illustrated that the sample included C, N, O, Fe, Cu, and also Na elements (Fig. 8, section **a**). The deconvoluted C 1s spectrum (Fig. 8, section **b**) showed binding energy peaks corresponding to C–H and C–C (284.74 eV), C–N (285.92 eV), and O=C–O (288.09 eV). Also, the deconvoluted N 1s spectrum (Fig. 8, section **c**) exhibited binding energy peaks corresponding to Cu–N (399.70 eV) and C–N (401.17 eV). Furthermore, the deconvoluted O 1s spectrum (Fig. 8, section **d**) presented binding energy peaks corresponding to Cu–O and Fe–O (529.62 eV), O*−C=O (531.07 eV), O* = C–O (531.75 eV), and H–O–H (535.31 eV). On the other hand, Fig. 8 (section **e**) shows that the Fe 2p spectrum can be mainly

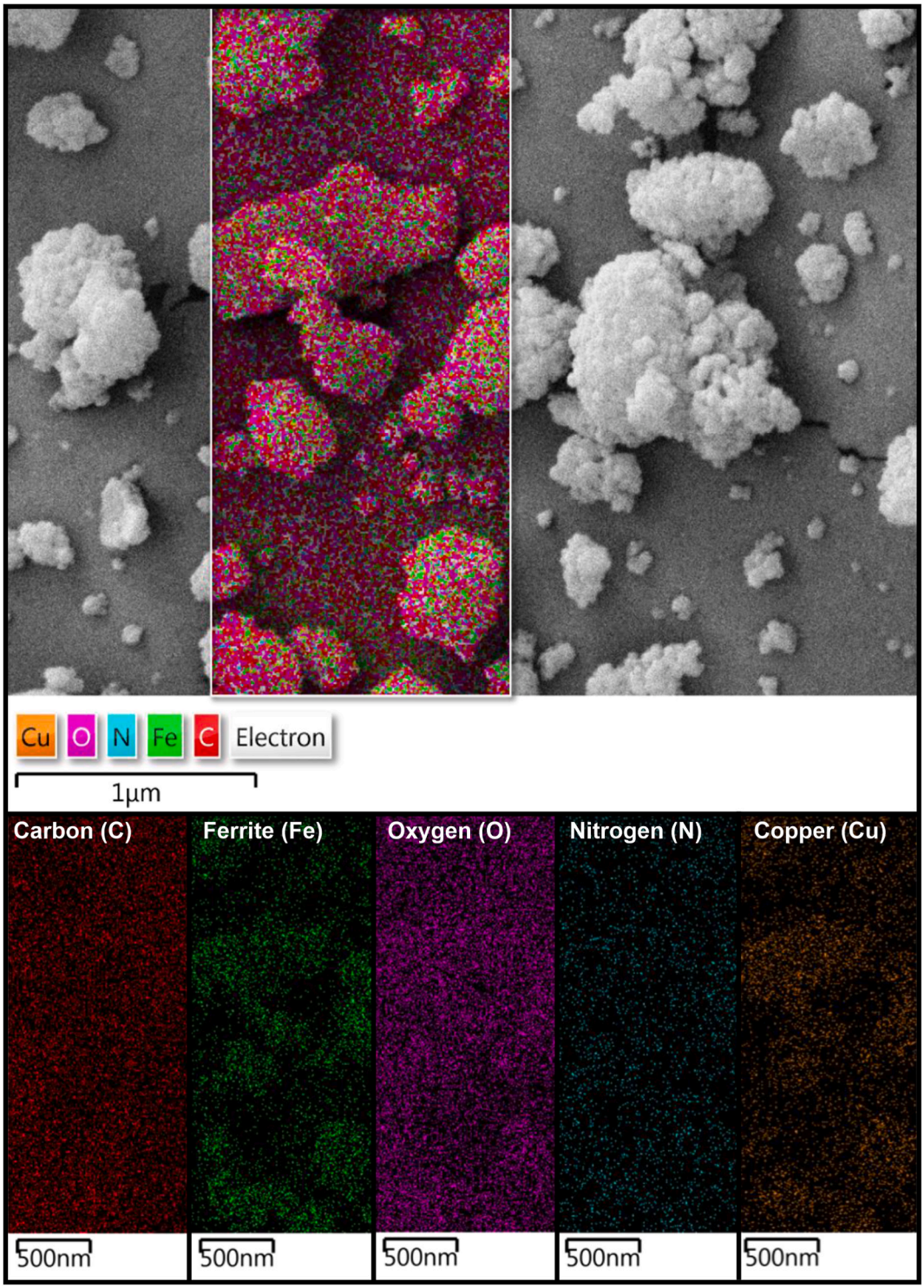


**Fig. 7.** SEM-based elemental mapping of the $Fe_3O_4$@EDTA@Cu(II) nanocomposite.

deconvoluted into Fe(II) $2p_{3/2}$ (710.06 eV), Fe(III) $2p_{3/2}$ (711.83 eV), Fe(II) $2p_{1/2}$ (723.70 eV), and Fe(III) $2p_{1/2}$ (725.62 eV). It is worthy to note the deconvoluted Cu 2p spectrum (Fig. 8, section **f**) revealed four distinct peaks at Cu(0) $2p_{3/2}$ (932.21 eV), Cu(II) $2p_{3/2}$ (933.80 eV), Cu(0) $2p_{1/2}$ (952.10 eV), and Cu(II) $2p_{1/2}$ (953.77 eV). Additionally, three satellite peaks at 941.02 ev, 943.70 eV, and 962.25 eV confirmed the present of CuO in the structure of the as-prepared $Fe_3O_4$@EDTA@Cu(II) nanocomposite (Fig. 8, section **f**)

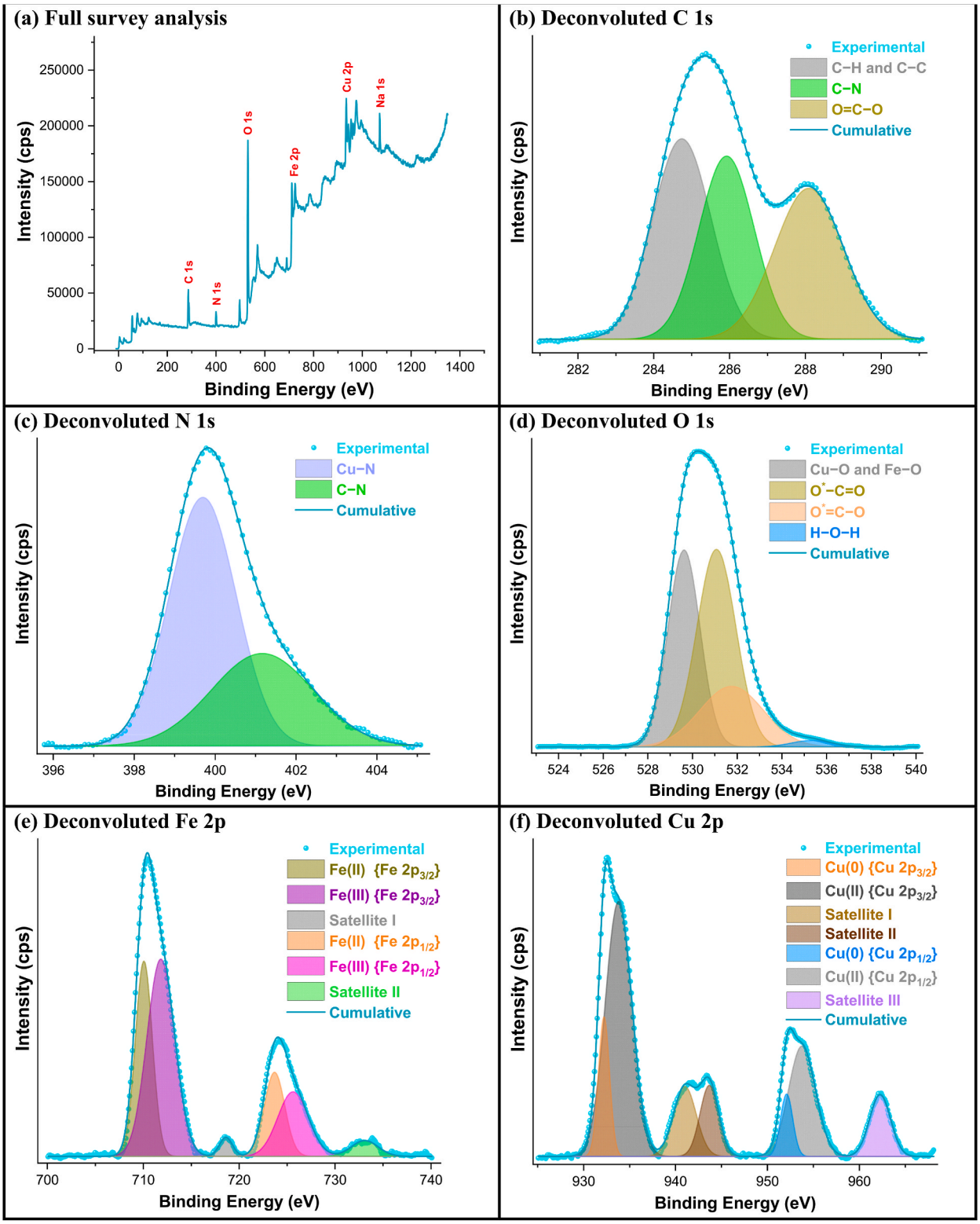


**Fig. 8.** XPS analysis of the as-prepared $Fe_3O_4$@EDTA@Cu(II) nanocomposite.

[52–55].

The magnetic properties of the prepared $Fe_3O_4$, $Fe_3O_4$@EDTA, and $Fe_3O_4$@EDTA@Cu(II) nanostructures were investigated at room temperature using the vibrating sample magnetometer (VSM) technique, as shown in Fig. 9. It is worthwhile to note that VSM is a widely used technique for studying magnetic materials and measuring their magnetic properties, including magnetic moment, magnetic anisotropy, and magnetic susceptibility. According to the VSM curves, the $Fe_3O_4$, $Fe_3O_4$@EDTA, and $Fe_3O_4$@EDTA@Cu(II) nanostructures exhibit superparamagnetic behavior with saturation magnetization (*Ms*) amounts of 64.49 emu $g^{-1}$, 21.62 emu $g^{-1}$, and 8.36 emu $g^{-1}$, respectively.

The thermal gravimetric analysis (TGA) was conducted to investigate the thermal stability of the as-prepared $Fe_3O_4$@EDTA@Cu(II) nanocomposite by heating it up to 700 °C (Fig. 10). The mentioned TGA diagram exhibits a weigh loss of around 2 % below 231 °C, which is related to the moisture content of the Cu(II)-containing nanocomposite. The second mass loss in the range of 240–400 °C is attributed to the thermal decomposition of EDTA.

The nitrogen ($N_2$) gas adsorption–desorption analysis of the $Fe_3O_4$@EDTA@Cu(II) nanocomposite confirmed the isotherm shape is IV with a $H_3$ hysteresis loop (Fig. 11, section **a**), which is characterized as mesoporous materials. Furthermore, from the BET plot (Fig. 11, section **b**), the specific surface area, pore volume value, and mean pore diameter of the as-prepared Cu(II)-containing mesoporous nanocomposite were 12.544 $m^2$ $g^{-1}$, 2.882 $cm^3$(STP) $g^{-1}$, and 12.12 nm, respectively. Also, the BJH pore size distribution plot of the titled $Fe_3O_4$@EDTA@Cu(II) nanocomposite is shown in Fig. 11 (section **c**).

### 2.2. Catalytic applications of the as-prepared $Fe_3O_4$@EDTA@Cu(II) nanocomposite

#### 2.2.1. Reduction of nitroarenes catalyzed by $Fe_3O_4$@EDTA@Cu(II) nanocomposite

First of all, the catalytic performance of the as-prepared $Fe_3O_4$@EDTA@Cu(II) nanocomposite (8 mg) was assessed on the reduction of nitrobenzene ($PhNO_2$) using sodium borohydride ($NaBH_4$) in various solvents and temperatures (Table 1). It is worthy to note that among various inorganic hydrides, $NaBH_4$ known as one of the most studies, simplest, mild hydrogen-rich chemical species for hydrogen production and reducing functional groups in organic synthesis [56–59]. The optimization process was carried out using different solvents, and the obtained results are reported in Table 1. As shown in Table 1, the suitable solvent and temperature for the mentioned model reaction were water and 60 °C, respectively. After that, the scope and limitations of the mentioned strategy were evaluated upon various aromatic nitro compounds, and the findings are illustrated in Table 2. This study showed that a small quantity of $Fe_3O_4$@EDTA@Cu(II) could achieve high performance in the stated reaction within a short period. Furthermore, the plausible reaction mechanism for the green reduction of aromatic nitro compounds using $NaBH_4$ in the presence of the as-prepared $Fe_3O_4$@EDTA@Cu(II) nanocomposite in water as is depicted in Scheme 1. In the first step, $NaBH_4$ dissociated in water to generate hydrogen gas ($H_2$) in the presence of the mentioned Cu(II)-containing mesoporous nanocatalyst, which we observed as bubbles inside the reaction vessel during the stated reaction. Then, the produced $H_2$ gas diffuses into the reaction environment and subsequently adsorbs onto the $Fe_3O_4$@EDTA@Cu(II) nanocomposite, especially on the Cu(II) nanoparticles surface. The activation of $H_2$ gas by $Fe_3O_4$@EDTA@Cu(II) nanocomposite is one of the fundamental steps in the reaction mechanism of nitroarenes reductions.

#### 2.2.2. One-pot reductive acetylation of nitroarenes and also N-acetylation of arylamines catalyzed by $Fe_3O_4$@EDTA@Cu(II) nanocomposite

In the next step, the potential catalytic application of the as-prepared $Fe_3O_4$@EDTA@Cu(II) nanocomposite in organic synthesis was investigated towards one-pot reductive acetylation of nitroarenes. The amide bond creation via a simple strategy has a special place in organic synthesis. The *N*-acetylation of arylamines is a widely recognized reaction in the field of organic synthesis, which serves as a means to protect amine functional groups in complex syntheses and prepare organic frameworks that contain acetamide

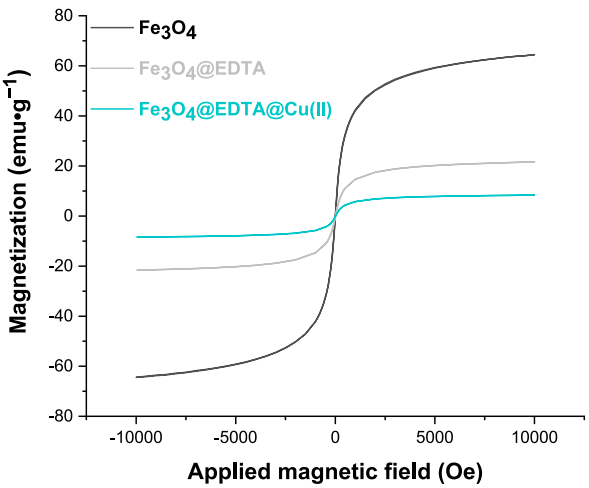


**Fig. 9.** Magnetization curves of the prepared $Fe_3O_4$, $Fe_3O_4$@EDTA, and $Fe_3O_4$@EDTA@Cu(II) nanostructures.

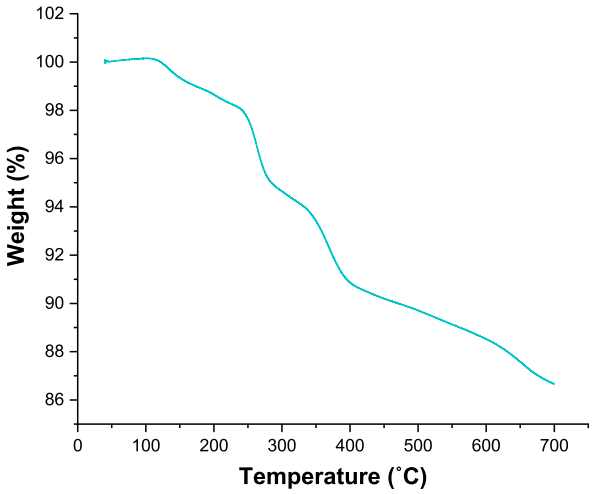


**Fig. 10.** TGA diagram of the as-prepared $Fe_3O_4$@EDTA@Cu(II) nanocomposite.

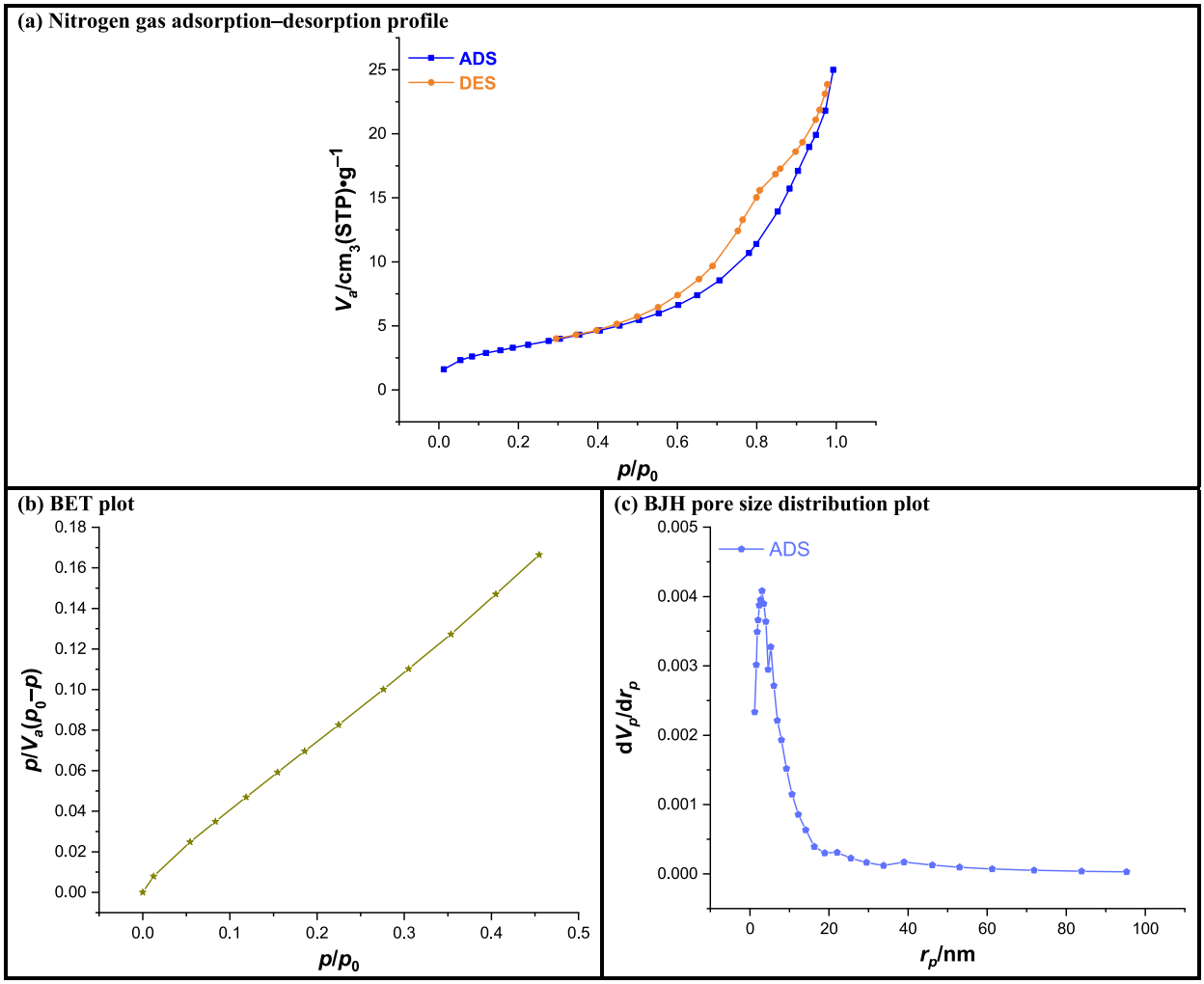


**Fig. 11.** Nitrogen gas adsorption–desorption profile (a), BET plot (b), and BJH pore size distribution plot (c) of the as-prepared $Fe_3O_4$@EDTA@Cu (II) nanocomposite.

**Table 1**
Optimization experiments for the reduction of $PhNO_2$ to $PhNH_2$ with $NaBH_4$ catalyzed by as-prepared $Fe_3O_4$@EDTA@Cu(II) nanocomposite.

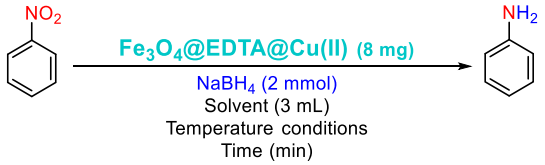


| Entry | Solvent | Temperature conditions | Time (min) | Conversion (%) |
|---|---|---|---|---|
| 1 | $H_2O$ | Room temperature | 60 | 45 |
| 2 | $H_2O$ | 60 °C | 6 | 100 |
| 5 | $CH_3OH$ | Reflux | 120 | 50 |
| 6 | $CH_3CH_2OH$ | Reflux | 120 | 40 |
| 7 | $CH_3CN$ | Reflux | 120 | 10 |
| 8 | $CH_2Cl_2$ | Reflux | 120 | 10 |
| 9 | PEG-400 | 60 °C | 120 | 30 |

moiety. It is worth noting that ongoing research endeavors continue to seek improvements in this uncomplicated chemical process. On the other hand, due to the importance of the one-pot reaction in synthetic chemistry and especially green chemistry [60–69], using the mentioned strategy for the stated one-pot reductive acetylation of nitroarenes is desirable. In this regard, and after obtaining the successful reduction strategy for the green reduction and conversion nitroarenes to the corresponding arylamines, we decided to introduce a new one-pot reductive acetylation approach for the efficient synthesis of *N*-arylacetamides from aromatic nitro compounds. To this purpose, in the second step of the stated one-pot organic reaction (viz. acetylation), we used 1 mmol of acetic anhydride ($Ac_2O$) as an acetylating agent under the same temperature conditions (60 °C). As shown in Table 3, we successfully prepared diverse *N*-arylacetamide derivatives. On the other hand, we tested the straightforward *N*-acetylation of arylamines in the presence of the as-prepared Cu(II)-containing nanocatalytic system in water using $Ac_2O$, and the obtained results illustrated in Table 4. The mentioned reaction, as shown in Table 4, revealed the rate of the acetylation reaction is swift and immediate. In addition, a suitable mechanism for this straightforward organic transformation is illustrated in Scheme 2.

### 2.3. Recoverability and reusability experiments of the as-prepared $Fe_3O_4$@EDTA@Cu(II) nanocomposite

The recyclability and reusability of the as-prepared $Fe_3O_4$@EDTA@Cu(II) nanocomposite have also been evaluated on the reduction of $PhNO_2$ (1 mmol) to $PhNH_2$ using $NaBH_4$ (2 mmol) in the presence of the as-prepared Cu(II)-containing mesoporous nanocatalyst (8 mg) in water at 60 °C as a model reaction, exposed satisfying results even after five runs (Fig. 12, section **a**). Moreover, a TEM image (Fig. 12, section **b**) of the recovered $Fe_3O_4$@EDTA@Cu(II) nanocomposite after the fourth recycling step has been demonstrated, which shows that the structure of the mentioned $Fe_3O_4$@EDTA@Cu(II) mesoporous nanocomposite remained intact.

### 2.4. A comparative study

To validate the efficiency of our new synthetic protocols on the reduction and one-pot reductive acetylation of nitroarenes in the presence of the as-prepared $Fe_3O_4$@EDTA@Cu(II) nanocomposite in water, both of them have been compared with some of the previously reported procedures. As shown in Table 5, the obtained results demonstrated that the current synthetic approaches have a convenient place in terms of efficiency and greenness than the previously available procedures.

## 3. Experimental

### 3.1. Reagents, samples, and apparatus

All starting materials, reagents, and solvents were commercially available and purchased from Merck, Sigma-Aldrich, and Fluka companies. SOLTEC SONICA 2400 MH S3 (300 W) instrument was used for ultrasonic irradiation. FT-IR spectra were recorded on Thermo Nicolet Nexus 670 spectrometer, and $^1$H NMR spectra were obtained by Bruker Avance 300 MHz spectrometer. The crystalline structures of the prepared nanocomposites were analyzed by X-ray diffraction (XRD) on a Philips PANalytical X'PertPro diffractometer (Netherlands) in 40 kV and 30 mA with a monochromatized Cu Kα radiation ($\lambda = 1.5418$ Å). SEM images and EDX diagram obtained from FESEM-TESCAN MIRA3 electronic microscope. TEM images were obtained from Zeiss EM10C-100 kV transmission electron microscope. X-ray photoelectron spectroscopy (XPS) analysis was performed using the SPECS UHV analysis system. Thermal gravimetric analysis (TGA) was performed using a TA Q600 device manufactured in the USA, over a temperature range of 40–700 °C. Magnetic properties of the prepared samples were measured using a vibrating sample magnetometer (Meghnatis Daghigh, Iran) under magnetic fields up to 20 kOe. The nitrogen adsorption–desorption isotherms were examined on Belsorp-Max, Japan.

**Table 2**
Reduction of nitroarenes to corresponding aryl amines using $NaBH_4$ catalyzed by as-prepared $Fe_3O_4$@EDTA@Cu(II) nanocomposite in water.

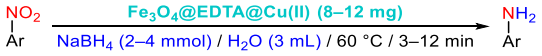


| Entry | Substrate | Product | RMCR | Time (min) | Yield (%) |
|---|---|---|---|---|---|
| 1 | 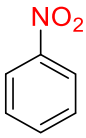 | 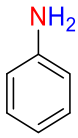 | 1:2:8 | 6 | 97 |
| 2 | 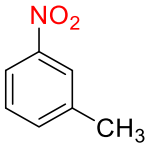 | 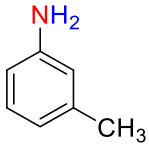 | 1:2:8 | 8 | 92 |
| 3 | 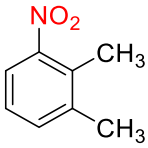 | 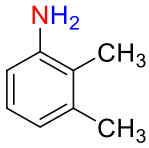 | 1:2:8 | 5 | 90 |
| 4 | 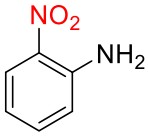 | 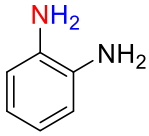 | 1:2:8 | 6 | 90 |
| 5 | 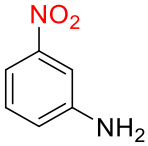 | 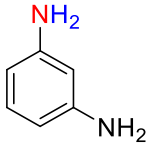 | 1:2:8 | 12 | 90 |
| 6 | 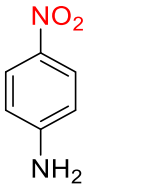 | 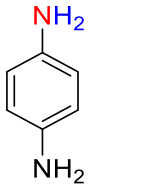 | 1:2:8 | 4 | 90 |
| 7 | 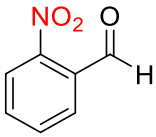 | 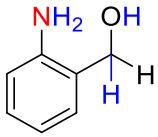 | 1:4:12 | 3 | 92 |
| 8 | 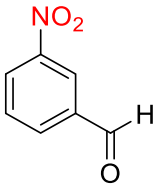 | 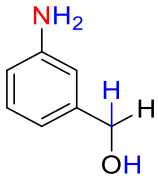 | 1:4:12 | 4 | 94 |

(*continued on next page*)

**Table 2** (*continued*)

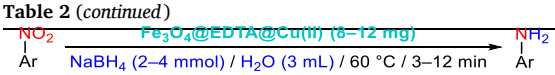


| Entry | Substrate | Product | RMCR | Time (min) | Yield (%) |
|---|---|---|---|---|---|
| 9 | 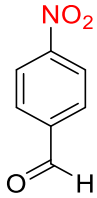 | 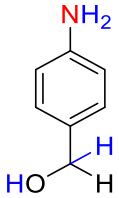 | 1:4:12 | 3 | 92 |
| 10 | 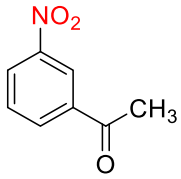 | 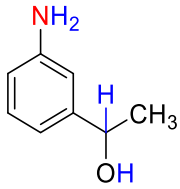 | 1:4:12 | 4 | 92 |
| 11 | 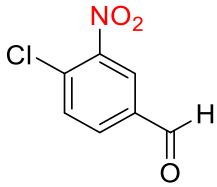 | 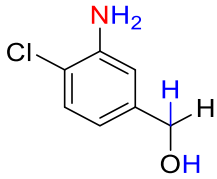 | 1:4:12 | 4 | 94 |
| 12 | 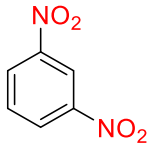 | 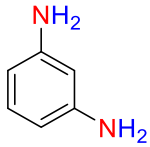 | 1:4:12 | 10 | 90 |

RMCR (Reaction main components ratio) = substrate (mmol):$NaBH_4$ (mmol):catalyst (mg).

### 3.2. Preparation of the $Fe_3O_4$@EDTA@Cu(II) nanocomposite

According to previous research, using a co-precipitation technique, black and dark-colored magnetite nanoparticles (MNPs) were effectively synthesized. The synthesis process involved mixing $FeCl_3{\cdot}6H_2O$ and $FeCl_2{\cdot}4H_2O$ in an alkaline medium under inert conditions. Then, 0.6 g of $Fe_3O_4$ nanoparticles were ultrasonicated in dichloromethane solvent to create a homogeneous mixture. Then, 0.6 g of EDTA disodium was added to the mixture and stirred at room temperature for 24 h to allow the EDTA to bind to the $Fe_3O_4$ nanoparticles. As a result, a brown color product was formed, which was then collected using a magnet. The product was washed three times with ethanol to remove any remaining impurities and dried. In the next step, the obtained $Fe_3O_4$@EDTA was ultrasonicated in ethanol to form a homogeneous solution, and approximately 0.7 g of pure copper powder was added to this solution. The mixture was then refluxed for 24 h, which enabled the Cu(II) ions to bind to the $Fe_3O_4$@EDTA nanocomposite. The resulting nanocomposite was then dried at 60 $^{o}$C, which removed any remaining solvent and left behind it.

### 3.3. General procedure for the reduction of nitroarenes to the corresponding arylamines catalyzed by $Fe_3O_4$@EDTA@Cu(II) nanocomposite

For example, in a round-bottom flask (10 mL) equipped with a magnetic stirrer, a mixture of $PhNO_2$ (1 mmol) and $H_2O$ (3 mL) was prepared. Then, the as-prepared $Fe_3O_4$@EDTA@Cu(II) nanocomposite (8 mg) was added, and the mixture was stirred. At the next step, $NaBH_4$ (2 mmol) was added, and the resulting mixture continued to stir at 60 °C for the appropriate time under oil-bath conditions. After completion of the reaction, the mixture was cooled to room temperature, and the mentioned Cu(II)-containing mesoporous nanocatalytic system was separated from the reaction pot by an external magnet. The reaction mixture was extracted with ethyl acetate (EtOAc) (2 × 5 mL) and then dried over anhydrous sodium sulfate ($Na_2SO_4$). Finally, the solvent was evaporated under reduced pressure to afford the pure liquid aniline in 97 % yield.

### 3.4. General procedure for the one-pot reductive acetylation of nitroarenes catalyzed by $Fe_3O_4$@EDTA@Cu(II) nanocomposite

As an example, and after completion of the $PhNO_2$ reduction process (which was completely discussed in **3.3** section), acetic anhydride ($Ac_2O$) (1 mmol) was added to the reaction mixture, followed by stirring for an additional 1 min at the same temperature.

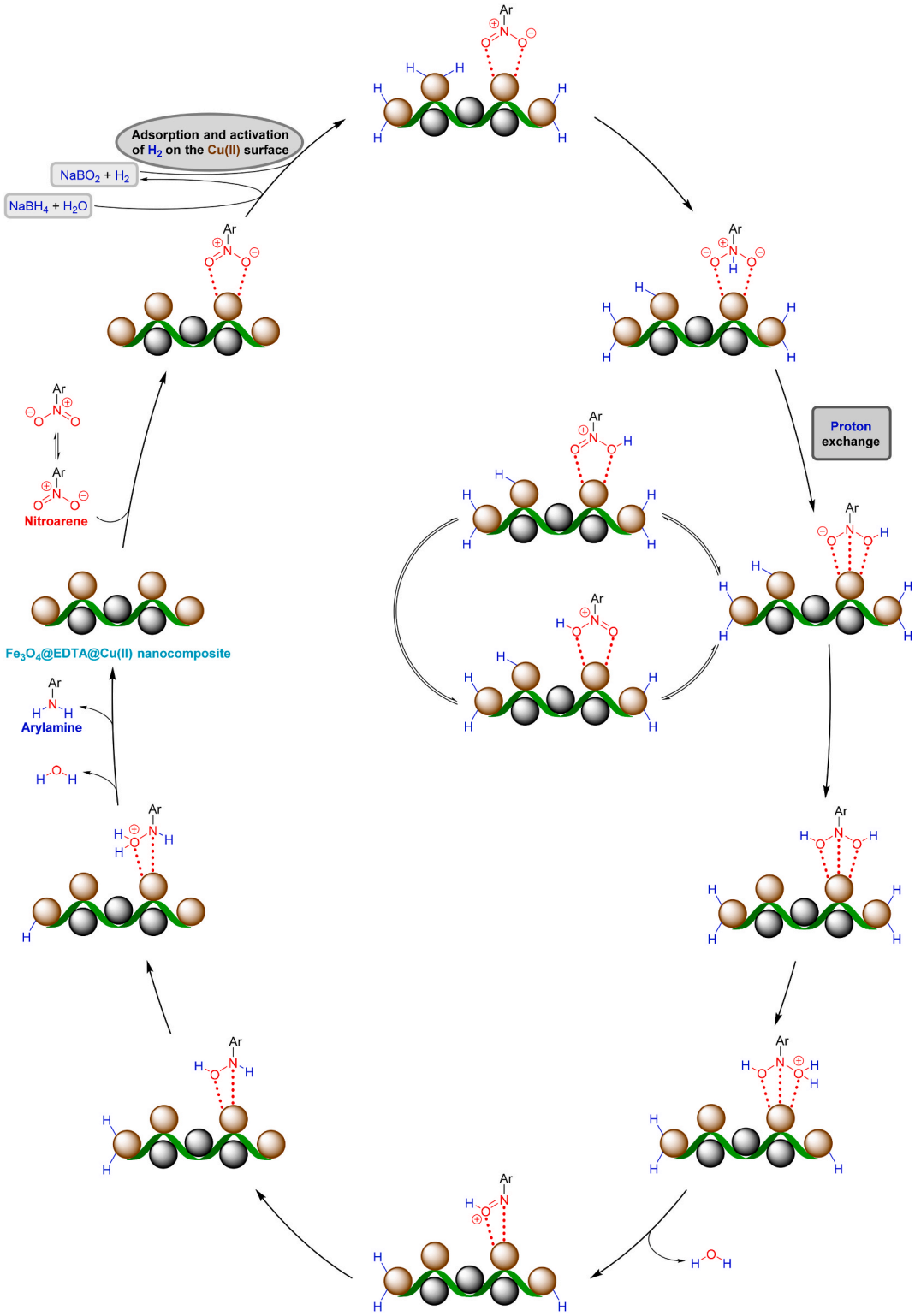


**Scheme 1.** Plausible mechanism for the $Fe_3O_4$@EDTA@Cu(II)-catalyzed reduction of $ArNO_2$ to $ArNH_2$ using $NaBH_4$.

Then, the mixture was cooled to room temperature, and the $Fe_3O_4$@EDTA@Cu(II) mesoporous nanocatalyst was separated using an external magnet. Then, the reaction mixture was extracted with EtOAc (2 × 5 mL) and then dried over anhydrous $Na_2SO_4$. Finally, evaporation of the solvent under reduced pressure afforded the pure acetanilide in 95 % yield.

**Table 3**
One-pot reductive acetylation of nitroarenes catalyzed by as-prepared $Fe_3O_4$@EDTA@Cu(II) nanocomposite in water.

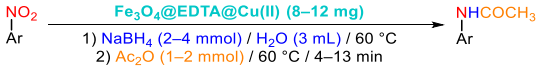


| Entry | Substrate | Product | RMCR | Time (min) | Yield (%) |
|---|---|---|---|---|---|
| 1 | 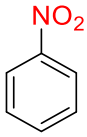 | 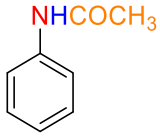 | 1:2:8:1 | 7 | 95 |
| 2 | 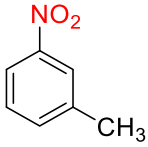 | 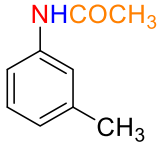 | 1:2:8:1 | 9 | 84 |
| 3 | 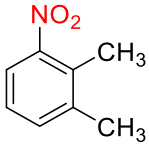 | 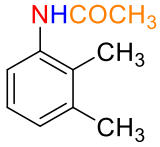 | 1:2:8:1 | 6 | 85 |
| 4 | 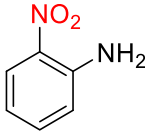 | 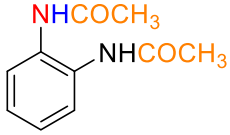 | 1:2:8:2 | 7 | 86 |
| 5 | 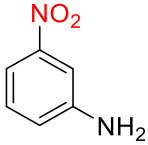 | 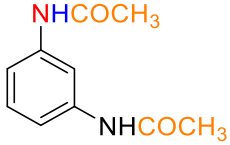 | 1:2:8:2 | 13 | 88 |
| 6 | 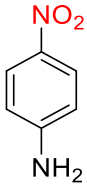 | 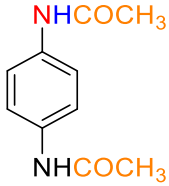 | 1:2:8:2 | 5 | 89 |
| 7 | 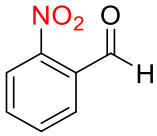 | 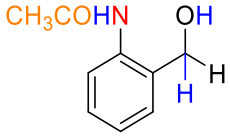 | 1:4:12:1 | 4 | 90 |
| 8 | 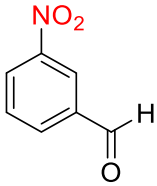 | 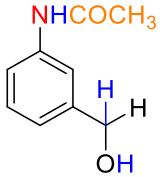 | 1:4:12:1 | 5 | 91 |

(*continued on next page*)

**Table 3** (*continued*)

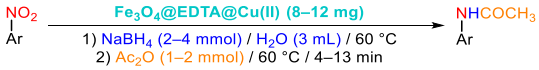


| Entry | Substrate | Product | RMCR | Time (min) | Yield (%) |
|---|---|---|---|---|---|
| 9 | 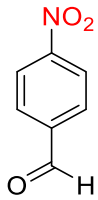 | 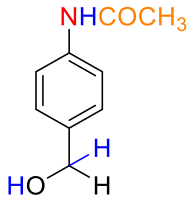 | 1:4:12:1 | 4 | 91 |
| 10 | 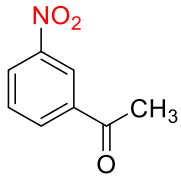 | 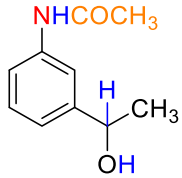 | 1:4:12:1 | 5 | 91 |
| 11 | 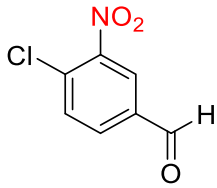 | 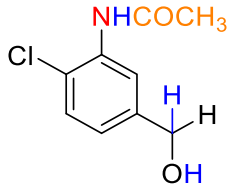 | 1:4:12:1 | 5 | 93 |
| 12 | 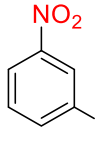 | 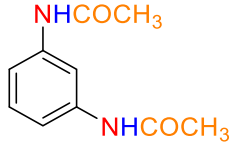 | 1:4:12:2 | 11 | 95 |

RMCR (Reaction main components ratio) = substrate (mmol):$NaBH_4$ (mmol):catalyst (mg):$Ac_2O$ (mmol).

### 3.5. Selected spectral data of products

#### 3.5.1. Aniline

FT-IR (KBr): 3429, 3352, 3210, 3071, 3035, 2926, 2850, 1620, 1601, 1498, 1467, 1276, 1149, 1021, 880, 752, 692, 503 $cm^{-1}$. $^1H$ NMR (300 MHz, $CDCl_3$): 7.20 (t, $J = 7.5$ Hz, 2H, Ar), 6.80 (t, $J = 7.2$ Hz, 1H, Ar), 6.72 (d, $J = 7.8$ Hz, 2H, Ar), 3.60 (bs, 2H, $NH_2$).

#### 3.5.2. Benzene-1,4-diamine

FT-IR (KBr): 3408, 3373, 3306, 3007, 2921, 1627, 1516, 1448, 1339, 1308, 1261, 1126, 1064, 1042, 932, 828, 714, 513 $cm^{-1}$. $^1H$ NMR (300 MHz, $CDCl_3$): 6.57 (s, 4H, Ar), 3.33 (bs, 4H, $NH_2$).

#### 3.5.3. (2-Aminophenyl)methanol

FT-IR (KBr): 3389, 3297, 3186, 3120, 3026, 2955, 2849, 1609, 1589, 1495, 1456, 1347, 1322, 1268, 1217, 1155, 1074, 1040, 1004, 932, 767, 750, 687, 609, 561, 532 $cm^{-1}$. $^1H$ NMR (300 MHz, $CDCl_3$): 7.13 (t, $J = 7.8$ Hz, 1H, Ar), 7.03 (d, $J = 7.5$ Hz, 1H, Ar), 6.75-6.65 (m, 2H, Ar), 4.59 (s, 2H, $CH_2$), 3.55 (s, 3H, $NH_2$ and OH).

#### 3.5.4. N-phenylacetamide

FT-IR (KBr): 3299, 3195, 3128, 2927, 1663, 1605, 1521, 1380, 1310, 1255, 1021, 815, 750, 610, 499 $cm^{-1}$. $^1H$ NMR (300 MHz, $CDCl_3$) 7.52 (s, 1H, —NH—), 7.49–7.27 (m, 4H, Ph), 7.11 (t, $J = 7.2$ Hz, 1H, Ph), 2.18 (s, 3H, —$CH_3$).

#### 3.5.5. N,N'-(1,4-phenylene)diacetamide

FT-IR (KBr): 3303, 3179, 3092, 2927, 2859, 1658, 1501, 1399, 1323, 1260, 1163, 1016, 879, 830, 742, 596, 527, 476 $cm^{-1}$. $^1H$ NMR (300 MHz, DMSO-$d_6$): 9.82 (s, 2H, 2 × NH), 7.46 (s, 4H, Ar), 1.98 (s, 6H, 2 × $CH_3$).

**Table 4**
*N*-Acetylation of arylamines catalyzed by as-prepared $Fe_3O_4$@EDTA@Cu(II) nanocomposite in water.

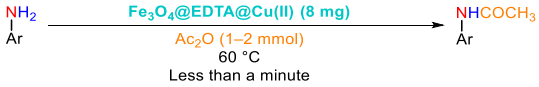


| Entry | Substrate | Product | RMCR | Yield (%) |
|---|---|---|---|---|
| 1 | 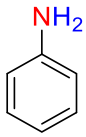 | 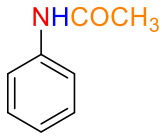 | 1:1 | 98 |
| 2 | 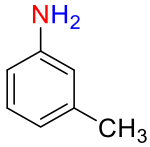 | 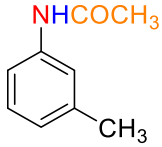 | 1:1 | 96 |
| 3 | 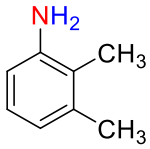 | 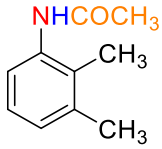 | 1:1 | 85 |
| 4 | 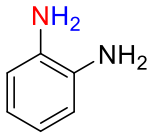 | 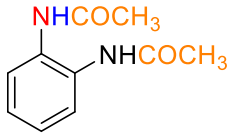 | 1:2 | 97 |
| 5 | 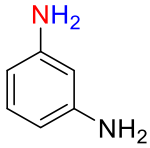 | 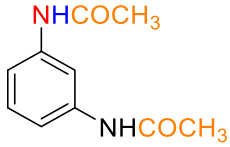 | 1:2 | 96 |
| 6 | 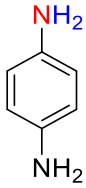 | 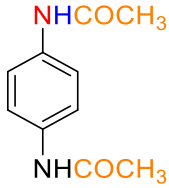 | 1:2 | 97 |
| 7 | 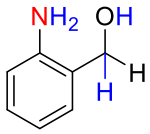 | 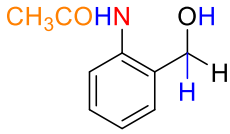 | 1:1 | 96 |
| 8 | 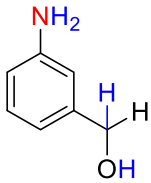 | 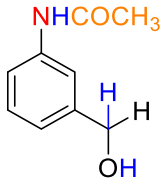 | 1:1 | 95 |

(*continued on next page*)

**Table 4** (*continued*)

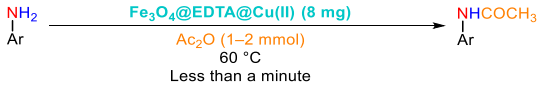


| Entry | Substrate | Product | RMCR | Yield (%) |
|---|---|---|---|---|
| 9 | 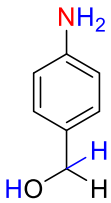 | 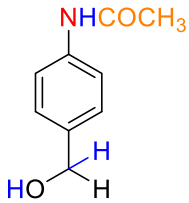 | 1:1 | 96 |
| 10 | 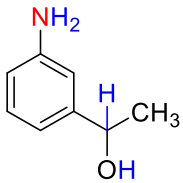 | 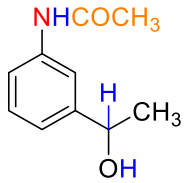 | 1:1 | 96 |
| 11 | 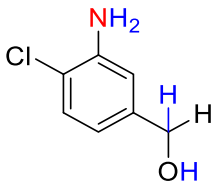 | 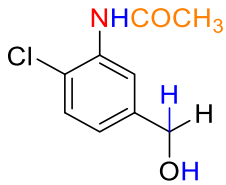 | 1:1 | 97 |
| 12 | 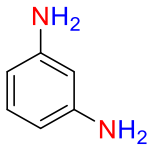 | 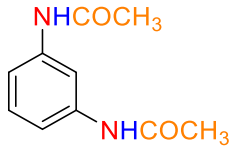 | 1:2 | 98 |

RMCR (Reaction main components ratio) = substrate (mmol):$Ac_2O$ (mmol).

## 4. Conclusion

Fundamentally, our research efforts were focused on developing efficient methods with minimal environmental impact for various organic transformations. To this purpose, we prepared a Cu(II)-containing mesoporous nanocatalytic system via a new strategy using copper metal powder instead of well-known copper salts. Subsequently, we characterized the structure of the mentioned as-prepared $Fe_3O_4$@EDTA@Cu(II) nanocomposite by FT-IR, XRD, SEM, TEM, SEM-based EDX and elemental mapping, XPS, TGA, VSM, and also BET and BJH analyses. Then, the mentioned $Fe_3O_4$@EDTA@Cu(II) mesoporous nanocomposite displayed satisfactory catalytic activity upon reduction and one-pot reductive acetylation of nitroarenes and also *N*-acetylation of arylamines in water at 60 °C. The large-scale nanosheets of the $Fe_3O_4$@EDTA@Cu(II) catalytic system possess a significant impact on the overall catalytic performance in the mentioned organic reactions. This particular heterogeneous catalyst promotes these reactions effectively. Its simplicity and ability to recover and reuse make it a cost-effective choice for practical applications. We also contribute to eco-friendly practices by using water as a solvent. The advantages of this approach are numerous. Not only do we achieve relatively short reaction times, but we also simplify the catalyst preparation using readily available resources at low cost. In addition, our synthetic strategies consistently produce valuable products with minimal purification. Overall, these innovative methods are promising for future applications in the chemical industry because they imply sustainable and efficient practical processes in chemistry.

## Consent for publication

Not applicable.

## Funding

This research received no specific grant from any funding agency in the public, commercial, or not-for-profit sectors.

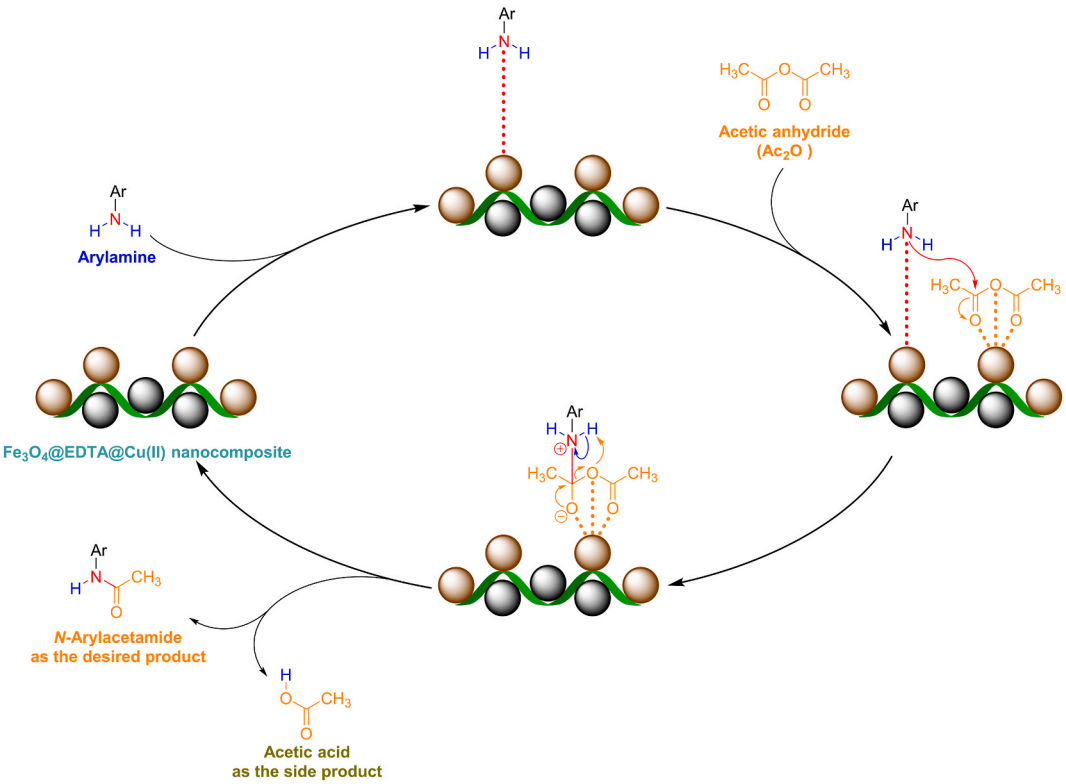


**Scheme 2.** Plausible mechanism for *N*-acetylation of arylamines catalyzed by $Fe_3O_4$@EDTA@Cu(II) nanocomposite.

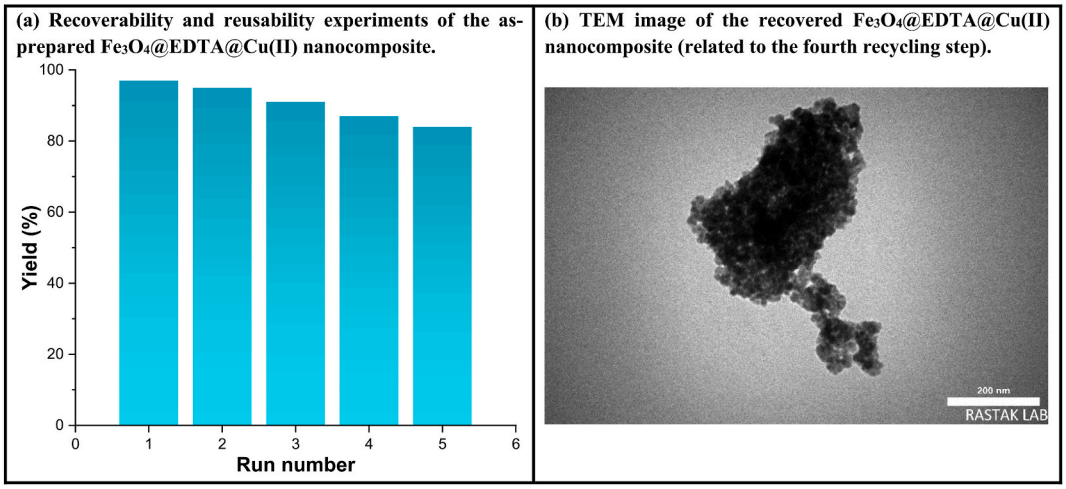


**Fig. 12.** Recoverability and reusability experiments (a) of the as-prepared $Fe_3O_4$@EDTA@Cu(II) nanocomposite and a TEM image (b) of the recovered Cu(II)-containing mesoporous nanocatalytic system.

## Data availability

Data will be made available on request.

## CRediT authorship contribution statement

**Leila Mavaddatiyan:** Writing – review & editing, Formal analysis, Conceptualization, Data curation, Investigation, Methodology, Resources, Software, Validation, Visualization, Writing – original draft. **Behzad Zeynizadeh:** Writing – review & editing,

**Table 5**
Comparison of the catalytic activity of the as-prepared $Fe_3O_4$@EDTA@Cu(II) nanocomposite with literature samples reported upon reduction and one-pot reductive acetylation of $PhNO_2$.

Part A

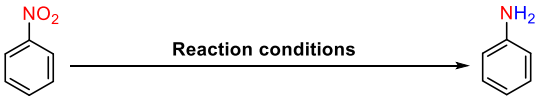


| Entry | Reaction conditions | Time | Yield | Ref. |
|---|---|---|---|---|
| A1 | $Fe_3O_4$@EDTA@Cu(II) (8 mg); $NaBH_4$ (2 mmol); $H_2O$; 60 °C | 6 min | 97 % | a |
| A2 | $Fe_3O_4$@$SiO_2$@KCC-1@MPTMS@$Cu^{II}$ (10 mg); $NaBH_4$ (2 mmol); $H_2O$; 60 °C | 5 min | 98 % | [47] |
| A3 | (7 wt%) Pd/C (30 mg); $NaBH_4$ (2 mmol); $H_2O$; reflux | 7 min | 93 % | [70] |
| A4 | $CuFe_2O_4$ (48 mg); $NaBH_4$ (2 mmol); $H_2O$; reflux | 50 min | 95 % | [71] |
| A5 | $Ni_2B$@$Cu_2O$ (54 mg); $NaBH_4$ (2.5 mmol); wet-solvent-free grinding; room temperature | 1 min | 98 % | [72] |
| A6 | $Ni_2B$@$CuCl_2$ (52 mg); $NaBH_4$ (2.5 mmol); wet-solvent-free grinding; room temperature | 2 min | 98 % | [72] |
| A7 | $Fe_2Se_2CO_9$ (3 mol%); $NH_2NH_2$•$H_2O$ (2 mmol); $H_2O$; 110 °C | 15 min | 89 % | [73] |
| A8 | $Ni(OH)_2$@PANI-1 (3.2 mol%); $NaBH_4$ (10 mmol); $H_2O$; reflux | 1.5 h | 85 % | [74] |
| A9 | Cu-BTC@$Fe_3O_4$ (15 mg); $NaBH_4$ (4 mmol); $CH_3CH_2OH$:$H_2O$ (3:1); 45 °C | 3 h | 99 % | [75] |
| A10 | IT-MHAP-Ag (60 mg); $NaBH_4$ (5 mmol); $H_2O$; reflux | 25 min | 98 % | [76] |
| A11 | PSeCN/Ag (20 mg); $NaBH_4$ (5 mmol); $H_2O$; 75 °C | 25 min | 99 % | [77] |
| A12 | $Fe_3O_4$@$SiO_2$@KIT-6@2-ATP@$Cu^{I}$ (20 mg); $NaBH_4$ (5 mmol); $H_2O$; r.t. | 60 min | 89 % | [78] |
| A13 | MBC-PVIm/Pd (30 mg); $NaBH_4$ (3 mmol); $H_2O$; 50 °C | 30 min | 99 % | [79] |
| A14 | $CuFe_2O_4$@$SiO_2$@PTMS@Tu@$Ni^{II}$ (20 mg); $NaBH_4$ (2 mmol); $H_2O$; 65 °C | 5 min | 96 % | [80] |
| A15 | Pd@CS-CD-MGQDs (6 mol%); $H_2$ (1 bar); deionized $H_2O$; 50 °C | 1 h | 97 % | [81] |
| A16 | $MoS_2$-rGO (10 mg); $NH_2NH_2$•$H_2O$ (1.5 mmol); $H_2O$; 100 °C | 2 h | 82 % | [82] |
| A17 | $Ni_2P$-AC (30 mg); $NH_2NH_2$•$H_2O$ (0.5 mL); Heptane; 70 °C | 2 h | 93 % | [83] |

**Part B**

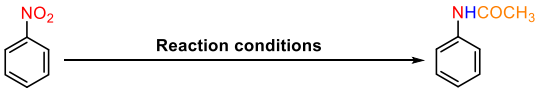


| **Entry** | **Reaction Conditions** | **Time** | **Yield** | **Ref.** |
|---|---|---|---|---|
| B1 | $Fe_3O_4$@EDTA@Cu(II) (5 mg); $NaBH_4$ (2 mmol); $Ac_2O$ (1 mmol); $H_2O$; 60 °C | 7 min | 95 % | a |
| B2 | $Fe_3O_4$@$SiO_2$@KCC-1@MPTMS@$Cu^{II}$ (10 mg); $NaBH_4$ (2 mmol); $Ac_2O$ (1 mmol); $H_2O$; 60 °C | 7 min | 95 % | [47] |
| B3 | (7 wt%) Pd/C (30 mg); $NaBH_4$ (2 mmol); $Ac_2O$ (1 mmol); $H_2O$; reflux | 8 min | 88 % | [70] |
| B4 | $Cu(Hdmg)_2$ (10 mol%); $NaBH_4$ (3 mmol); EtOAc; 60 °C | 170 min | 97 % | [43] |
| B5 | $CuFe_2O_4$ (48 mg); $NaBH_4$ (2 mmol); $Ac_2O$ (1 mmol); $H_2O$; reflux | 11 min | 97 % | [84] |
| B6 | $Ni_2B$@$Cu_2O$ (54 mg); $NaBH_4$ (2.5 mmol); $Ac_2O$ (1 mmol); wet-solvent-free grinding; 40 °C | 2 min | 97 % | [85] |
| B7 | $Ni_2B$@$CuCl_2$ (52 mg); $NaBH_4$ (2.5 mmol); $Ac_2O$ (1 mmol); wet-solvent-free grinding; 40 °C | 3 min | 97 % | [85] |
| B8 | $CuFe_2O_4$@$SiO_2$@PTMS@Tu@$Ni^{II}$ (20 mg); $NaBH_4$ (2 mmol); $Ac_2O$ (1 mmol); $H_2O$; 65 °C | 7 min | 94 % | [80] |
| B9 | (2 wt%) Pd/(5 wt%) Sn–$Al_2O_3$ (50 mg); $H_2$ atmosphere; $Ac_2O$ (1 mmol); $H_2O$; room temperature | 3 h | 98 % | [86] |

[a] Present work.

Conceptualization, Data curation, Funding acquisition, Methodology, Project administration, Resources, Supervision, Validation.

## Declaration of competing interest

The authors declare that they have no known competing financial interests or personal relationships that could have appeared to influence the work reported in this paper.

## Acknowledgement

The authors gratefully appreciate the financial support of this work by Research Council of Urmia University.

## References

[1] J.B. Zimmerman, P.T. Anastas, H.C. Erythropel, W. Leitner, Designing for a green chemistry future, Science 367 (2020) 397–400, https://doi.org/10.1126/science.aay3060.
[2] H.C. Erythropel, J.B. Zimmerman, T.M. de Winter, L. Petitjean, F. Melnikov, C.H. Lam, A.W. Lounsbury, K.E. Mellor, N.Z. Janković, Q. Tu, L.N. Pincus, M. M. Falinski, W. Shi, P. Coish, D.L. Plata, P.T. Anastas, The Green ChemisTREE: 20 years after taking root with the 12 principles, Green Chem. 20 (2018) 1929–1961, https://doi.org/10.1039/C8GC00482J.
[3] T. Keijer, V. Bakker, J.C. Slootweg, Circular chemistry to enable a circular economy, Nat. Chem. 11 (2019) 190–195, https://doi.org/10.1038/s41557-019-0226-9.
[4] H. Mousavi, A comprehensive survey upon diverse and prolific applications of chitosan-based catalytic systems in one-pot multi-component synthesis of heterocyclic rings, Int. J. Biol. Macromol. 186 (2021) 1003–1166, https://doi.org/10.1016/j.ijbiomac.2021.06.123.
[5] M. Rimaz, Z. Jalalian, H. Mousavi, R.H. Prager, Base organocatalyst mediated annulation of arylglyoxalmonohydrates with 2,4-dihydroxyquinoline to form new pyranodiquinolinones, Tetrahedron Lett. 57 (2016) 105–109, https://doi.org/10.1016/j.tetlet.2015.11.074.

[6] N. Khaleghi, M. Esmkhani, M. Noori, N. Dasyafteh, M. Khalili Ghomi, M. Mahdavi, M.H. Sayahi, S. Javanshir, Copper supported modified magnetic carrageenan as a bio-based catalyst for the synthesis of novel scaffolds bearing the 1,2,3-triazole unit through the click reaction, Nanoscale Adv. 6 (2024) 2337–2349, https://doi.org/10.1039/D4NA00022F.

[7] M. Rimaz, H. Mousavi, P. Keshavarz, B. Khalili, $ZrOCl_2.8H_2O$ as a green and efficient catalyst for the expeditious synthesis of substituted 3-arylpyrimido[4,5-*c*]pyridazines in water, Curr. Chem. Lett. 4 (2015) 159–168, https://doi.org/10.5267/j.ccl.2015.6.001.

[8] C. Capello, U. Fischer, K. Hungerbühler, What is a green solvent? a comprehensive framework for the environmental assessment of solvents, Green Chem. 9 (2007) 927–934, https://doi.org/10.1039/B617536H.

[9] C.J. Clarke, W.-C. Tu, O. Levers, A. Bröhl, J.P. Hallett, Green and sustainable solvents in chemical processes, Chem. Rev. 118 (2018) 747–800, https://doi.org/10.1021/acs.chemrev.7b00571.

[10] M.-O. Simon, C.-J. Li, Green chemistry oriented organic synthesis in water, Chem. Soc. Rev. 41 (2012) 1415–1427, https://doi.org/10.1039/C1CS15222J.

[11] H. Mousavi, B. Zeynizadeh, M. Rimaz, Green and efficient one-pot three-component synthesis of novel drug-like furo[2,3-*d*]pyrimidines as potential active site inhibitors and putative allosteric hotspots modulators of both SARS-CoV-2 $M^{Pro}$ and $PL^{Pro}$, Bioorg. Chem. 135 (2023) 106390, https://doi.org/10.1016/j.bioorg.2023.106390.

[12] B. Zeynizadeh, H. Mousavi, F. Mohammad Aminzadeh, A hassle-free and cost-effective transfer hydrogenation strategy for the chemoselective reduction of arylnitriles to primary amines through in situ-generated $nickel^{II}$ dihydride intermediate in water, J. Mol. Struct. 1255 (2022) 131926, https://doi.org/10.1016/j.molstruc.2021.131926.

[13] M. Rimaz, J. Khalafy, H. Mousavi, A green organocatalyzed one-pot protocol for efficient synthesis of new substituted pyrimido[4,5-*d*]pyrimidinones using a Biginelli-like reaction, Res. Chem. Intermed. 42 (2016) 8185–8200, https://doi.org/10.1007/s11164-016-2588-6.

[14] M. Rimaz, J. Khalafy, H. Mousavi, S. Bohlooli, B. Khalili, Two different green catalytic systems for one-pot regioselective and chemoselective synthesis of some pyrimido[4,5-*d*]pyrimidinone derivatives in water, J. Heterocycl. Chem. 54 (2017) 3174–3186, https://doi.org/10.1002/jhet.2932.

[15] I. Borthakur, S. Kumari, S. Kundu, Water as a solvent: transition metal catalyzed dehydrogenation of alcohols going green, Dalton Trans. 51 (2022) 11987–12020, https://doi.org/10.1039/D2DT01060G.

[16] P. Kovacic, R. Somanathan, Nitroaromatic compounds: environmental toxicity, carcinogenicity, mutagenicity, therapy and mechanism, J. Appl. Toxicol. 34 (2014) 810–824, https://doi.org/10.1002/jat.2980.

[17] S. Zhang, Q. Liu, L. Zhong, J. Jiang, X. Luo, X. Hu, Q. Liu, Y. Lu, *Geobacter sulfurreducens* promoted the biosynthesis of reduced graphene oxide and coupled it for nitrobenzene reduction, J. Environ. Sci. 138 (138) (2024) 458–469, https://doi.org/10.1016/j.jes.2023.04.009.

[18] N.Y. Baran, M. Çalişkan, A. Özpala, T. Baran, Fabrication of nano-sized Pd catalyst supported on sodium carboxymethyl cellulose/gum Arabic/sodium alginate functionalized microspheres for catalytic reduction of nitro compounds, organic dyes, $K_3[Fe(CN)_6]$, and chromium(VI) pollutants, Int. J. Biol. Macromol. 262 (2024) 130134, https://doi.org/10.1016/j.ijbiomac.2024.130134.

[19] A. Khalil, A. Khan, T. Kamal, A.A.P. Khan, S.B. Khan, M.T.S. Chani, K.A. Alzahrani, N. Ali, Zn/Al layered double hydroxide and carboxymethyl cellulose composite beads as support for the catalytic gold nanoparticles and their applications in the reduction of nitroarenes, Int. J. Biol. Macromol. 262 (2024) 129986, https://doi.org/10.1016/j.ijbiomac.2024.129986.

[20] N.Y. Baran, Highly efficient and reusable Pd nanoparticles decorated on a novel Schiff base polymer for reduction of nitroarenes and Suzuki coupling reactions, J. Organomet. Chem. 1008 (2024) 123047, https://doi.org/10.1016/j.jorganchem.2024.123047.

[21] J. Wu, W. Lang, H. Li, K. Du, J. Deng, S. Zhao, W. Zhang, Z. Peng, Z. Liu, Interfacial effect of CNT-supported ultrafine Ru nanoclusters on efficient transfer hydrogenation of nitroaromatic compounds, ACS Sustainable Chem. Eng. 11 (2023) 14960–14968, https://doi.org/10.1021/acssuschemeng.3c03383.

[22] J. Ma, X. Mao, C. Hu, X. Wang, W. Gong, D. Liu, R. Long, A. Du, H. Zhao, Y. Xiong, Highly efficient iron-based catalyst for light-driven selective hydrogenation of nitroarenes, J. Am. Chem. Soc. 146 (2024) 970–978, https://doi.org/10.1021/jacs.3c11610.

[23] A. Singh, O. Singh, A. Maji, S. Singh, N. Singh, P.K. Maji, K. Ghosh, Catalytic transfer hydrogenation of substituted nitro-aromatics through in-situ generated Co (0) nanoparticle from Co(II) complexes supported by pentadentate ligands, Mol. Catal. 555 (2024) 113835, https://doi.org/10.1016/j.mcat.2024.113835.

[24] S. Karimi, M. Gholinejad, R. Khezri, J.M. Sansano, C. Nájera, M. Yus, Gold and palladium supported on an ionic liquid modified Fe-based metal–organic framework (MOF) as highly efficient catalysts for the reduction of nitrophenols, dyes and Sonogashira–Hagihara reactions, RSC Adv. 13 (2023) 8101–8113, https://doi.org/10.1039/D3RA00283G.

[25] W. Gao, Y. Gao, B. Liu, J. kang, Z. Zhang, M. Zhang, Y. Zou, Nitrogen-doped carbon material NCM-*T* heterogeneously catalyzed liquid-phase hydrogenation of nitrobenzene to aniline, RSC Adv. 14 (2024) 5055–5060, https://doi.org/10.1039/D4RA00078A.

[26] I. Klopcic, M.S. Dolenc, Chemicals and drugs forming reactive quinone and quinone imine metabolites, Chem. Res. Toxicol. 32 (2018) 1–34, https://doi.org/10.1021/acs.chemrestox.8b00213.

[27] M.A. Holgado, J.L. Arias, M.J. Cózar, J. Alvarez-Fuentes, A.M. Gañán-Calvo, M. Fernández-Arévalo, Synthesis of lidocaine-loaded PLGA microparticles by flow focusing: effects on drug loading and release properties, Int. J. Pharm. 358 (2008) 27–35, https://doi.org/10.1016/j.ijpharm.2008.02.012.

[28] N.S. Suveges, R.O. de Souza, B. Gutmann, C.O. Kappe, Synthesis of mepivacaine and its analogues by a continuous-flow tandem hydrogenation/reductive amination strategy, Eur. J. Org. Chem. 2017 (2017) 6511–6517, https://doi.org/10.1002/ejoc.201700824.

[29] D. Razafimahefa, L. Pélinski, M.T. Martin, D. Ramanitrahasimbola, P. Rasoanaivo, J. Brocard, Synthesis and chloroquine-enhancing activity of $N_a$-deacetyl-ferrocenoyl-strychnobrasiline, Bioorg. Med. Chem. Lett 15 (2005) 1239–1241, https://doi.org/10.1016/j.bmcl.2004.11.067.

[30] X. Wu, Y. Yao, L. Wang, D. Zhou, F. Sun, J. Chen, R. Ji, Synthesis of typical sulfonamide antibiotics with [$^{14}$C]- and [$^{13}$C]-labeling on the phenyl ring for use in environmental studies, Environ. Sci. Eur. 34 (2022) 23, https://doi.org/10.1186/s12302-022-00598-z.

[31] A.V. Erkin, E.B. Serebryakov, V.I. Krutikov, 2-[(2-Amino-6-methylpyrimidin-4-yl)sulfanyl]-*N*-arylacetamides: discovery of a new class of anti-tubercular agents and prospects for their further structural modification, Bioorg. Med. Chem. Lett. 83 (2023) 129189, https://doi.org/10.1016/j.bmcl.2023.129189.

[32] R.E. Abdelwahab, M.A. Ragheb, A.H.M. Elwahy, I.A. Abdelhamid, A.M. Abdelmoniem, Conjugate and regiochemical addition of aminoazoles to 2-(4-(2,2-dicyanovinyl)phenoxy)-*N*-arylacetamide affording fused pyrimidines linked to phenoxy-*N*-arylacetamide: antibacterial activity, molecular docking, and DNA binding studies, J. Mol. Struct. 1307 (2024) 137946, https://doi.org/10.1016/j.molstruc.2024.137946.

[33] Z. Zhao, F. Li, W. Chen, Q. Yang, H. Lu, J. Zhang, Discovery of aromatic 2-(3-(methylcarbamoyl) guanidino)-*N*-aylacetamides as highly potent chitinase inhibitors, Bioorg. Med. Chem. Lett. 80 (2023) 117172, https://doi.org/10.1016/j.bmc.2023.117172.

[34] D. Wang, D. Astruc, Fast-growing field of magnetically recyclable nanocatalysts, Chem. Rev. 114 (2014) 6949–6985, https://doi.org/10.1021/cr500134h.

[35] S.H. Gebre, Recent developments of supported and magnetic nanocatalysts for organic transformations: an up-to-date review, Appl. Nanosci. 13 (2023) 15–63, https://doi.org/10.1007/s13204-021-01888-3.

[36] H. Veisi, M. Pirhayati, P. Mohammadi, T. Tamoradi, S. Hemmati, B. Karmakar, Recent advances in the application of magnetic nanocatalysts in multicomponent reactions, RSC Adv. 13 (2023) 20530–20556, https://doi.org/10.1039/D3RA01208E.

[37] N. Agarwal, V.S. Solanki, B. Pare, N. Singh, S.B. Jonnalagadda, Current trends in nanocatalysis for green chemistry and its applications- a mini-review, Curr. Opin. Green Sustainable Chem. 41 (2023) 100788, https://doi.org/10.1016/j.cogsc.2023.100788.

[38] B. Karimi, F. Mansouri, H.M. Mirzaei, Recent applications of magnetically recoverable nanocatalysts in C−C and C−X coupling reactions, ChemCatChem 7 (2015) 1736–1789, https://doi.org/10.1002/cctc.201403057.

[39] T. Zhao, J. Pan, C. Mao, L. Chen, J. Li, H. Shao, G. Xu, Enhanced decomplexation of Cu-EDTA and simultaneous removal of Cu(II) by electron beam irradiation accompanied with autocatalytic fenton-like reaction: synergistic performance and mechanism, Chemosphere 313 (2023) 137445, https://doi.org/10.1016/j.chemosphere.2022.137445.

[40] M.B. Gawande, A. Goswami, F.-X. Felpin, T. Asefa, X. Huang, R. Silva, X. Zou, R. Zboril, R.S. Varma, Cu and Cu-based nanoparticles: synthesis and applications in catalysis, Chem. Rev. 116 (2016) 3722–3811, https://doi.org/10.1021/acs.chemrev.5b00482.

[41] S.E. Allen, R.R. Walvoord, R. Padilla-Salinas, M.C. Kozlowski, Aerobic copper-catalyzed organic reactions, Chem. Rev. 113 (2013) 6234–6458, https://doi.org/10.1021/cr300527g.

[42] A.P. Shah, A.S. Sharma, S. Jain, N.G. Shimpi, Microwave assisted one pot three component synthesis of propargylamine, tetra substituted propargylamine and pyrrolo[1,2-*a*]quinolines using CuNPs@ZnO–PTh as a heterogeneous catalyst, New J. Chem. 42 (2018) 8724–8737, https://doi.org/10.1039/C8NJ00410B.

[43] B. Zeynizadeh, H. Mousavi, S. Zarrin, Application of $Cu(Hdmg)_2$ as a simple and cost-effective catalyst for the convenient one-pot reductive acetylation of aromatic nitro compounds, J. Chin. Chem. Soc. 66 (2019) 928–933, https://doi.org/10.1002/jccs.201800325.

[44] S. Kohli, G. Rathee, S. Hooda, R. Chandra, An efficient approach for the green synthesis of biologically active 2,3-dihydroquinazolin-4(1*H*)-ones using a magnetic EDTA coated copper based nanocomposite, RSC Adv. 13 (2023) 1923–1932, https://doi.org/10.1039/D2RA07496F.

[45] H. Mousavi, B. Zeynizadeh, M. Hasanpour Galehban, $Ni^{II}$-containing L-glutamic acid cross-linked chitosan anchored on $Fe_3O_4$/f-MWCNT: a sustainable catalyst for the green reduction and one-pot two-step reductive Schotten–Baumann-type acetylation of nitroarenes, Nanoscale Adv. 6 (2024) 3961–3977, https://doi.org/10.1039/d4na00160e.

[46] M. Hasanpour Galehban, B. Zeynizadeh, H. Mousavi, Introducing $Fe_3O_4$@$SiO_2$@KCC-1@MPTMS@$Cu^{II}$ catalytic applications for the green one-pot syntheses of 2-aryl(or heteroaryl)-2,3-dihydroquinazolin-4(1*H*)-ones and 9-aryl-3,3,6,6-tetramethyl-3,4,5,6,7,9-hexahydro-1*H*-xanthene-1,8(2*H*)-diones, J. Mol. Struct. 1271 (2023) 134017, https://doi.org/10.1016/j.molstruc.2022.134017.

[47] M. Hasanpour Galehban, B. Zeynizadeh, H. Mousavi, Diverse and efficient catalytic applications of new cockscomb flower-like $Fe_3O_4$@$SiO_2$@KCC-1@MPTMS@$Cu^{II}$ mesoporous nanocomposite in the environmentally benign reduction and reductive acetylation of nitroarenes and one-pot synthesis of some coumarin compounds, RSC Adv. 12 (2022) 11164–11189, https://doi.org/10.1039/D1RA08763K.

[48] M. Hasanpour Galehban, B. Zeynizadeh, H. Mousavi, $Ni^{II}$ NPs entrapped within a matrix of L-glutamic acid cross-linked chitosan supported on magnetic carboxylic acid-functionalized multi-walled carbon nanotube: a new and efficient multi-task catalytic system for the green one-pot synthesis of diverse heterocyclic frameworks, RSC Adv. 12 (2022) 16454–16478, https://doi.org/10.1039/D1RA08454B.

[49] B. Zeynizadeh, H. Mousavi, F. Sepehraddin, A green and efficient Pd-free protocol for the Suzuki–Miyaura cross-coupling reaction using $Fe_3O_4$@APTMS@$Cp_2ZrCl_{x(x\,=\,0,\,1,\,2)}$ MNPs in PEG-400, Res. Chem. Intermed. 46 (2020) 3361–3382, https://doi.org/10.1007/s11164-020-04145-4.

[50] B. Zeynizadeh, F. Sepehraddin, H. Mousavi, Green and highly efficient strategies for the straightforward reduction of carboxylic acids to alcohols using four different and affordable types of hydrogen donors, Ind. Eng. Chem. Res. 58 (2019) 16379–16388, https://doi.org/10.1021/acs.iecr.9b01847.

[51] F. Mohammad Aminzadeh, B. Zeynizadeh, Immobilized nickel boride nanoparticles on magnetic functionalized multi-walled carbon nanotubes: a new nanocomposite for the efficient one-pot synthesis of 1,4-benzodiazepines, Nanoscale Adv. 5 (2023) 4499–4520, https://doi.org/10.1039/D3NA00415E.

[52] M. Aghazadeh, I. Karimzadeh, M.R. Ganjali, D. Gharailou, S.M. Hamad, EDTA-grafted $Cu^{2+}$-doped superparamagnetic nanoparticles: facile novel synthesis and their structural and magnetic characterizations, Appl. Phys. 125 (2019) 506, https://doi.org/10.1007/s00339-019-2803-6.

[53] M.C. Biesinger, L.W.M. Lau, A.R. Gerson, R.S.C. Smart, Resolving surface chemical states in XPS analysis of first row transition metals, oxides and hydroxides: Sc, Ti, V, Cu and Zn, Appl. Surf. Sci. 257 (2010) 887–898, https://doi.org/10.1016/j.apsusc.2010.07.086.

[54] A. Kaphle, E. Echeverria, D.N. Mcllroy, P. Hari, Enhancement in the performance of nanostructured CuO–ZnO solar cells by band alignment, RSC Adv. 10 (2020) 7839–7854, https://doi.org/10.1039/C9RA10771A.

[55] X. Sun, F. Luo, Facile fabrication of large-area CuO flakes for sodium-ion energy storage applications, Molecules 29 (2024) 2528, https://doi.org/10.3390/molecules29112528.

[56] G.M. Bousada, V.N. da Silva, B.F. de Souza, R.S. de Oliveira, I.M. Junior, C.H.F. da Cunha, D. Astruc, R.R. Teixeira, R.P.L. Moreira, Niobic acid as a support for microheterogeneous nanocatalysis of sodium borohydride hydrolysis under mild conditions, RSC Adv. 14 (2024) 19459–19471, https://doi.org/10.1039/D4RA01879F.

[57] R.C. Wade, Catalyzed reduction of organofunctional groups with sodium borohydride, J. Mol. Catal. 18 (1983) 273–297, https://doi.org/10.1016/0304-5102(83)80110-2.

[58] G.W. Gribble, Sodium borohydride in carboxylic acid media: a phenomenal reduction system, Chem. Soc. Rev. 27 (1998) 395–404, https://doi.org/10.1039/A827395Z.

[59] N. Kang, R. Djeda, Q. Wang, F. Fu, J. Ruiz, L.-L. Pozzo, D. Astruc, Efficient "click"-dendrimer-supported synergistic bimetallic nanocatalysis for hydrogen evolution by sodium borohydride hydrolysis, ChemCatChem 11 (2019) 2341–2349, https://doi.org/10.1002/cctc.201900246.

[60] A. Dömling, W. Wang, K. Wang, Chemistry and biology of multicomponent reactions, Chem. Rev. 112 (2012) 3083–3135, https://doi.org/10.1021/cr100233r.

[61] H. Mousavi, M. Rimaz, B. Zeynizadeh, Practical three-component regioselective synthesis of drug-like 3-aryl(or heteroaryl)-5,6-dihydrobenzo[*h*]cinnolines as potential non-covalent multi-targeting inhibitors to combat neurodegenerative diseases, ACS Chem. Neurosci. 15 (2024) 1828–1881, https://doi.org/10.1021/acschemneuro.4c00055.

[62] M. Rimaz, H. Mousavi, L. Nikpey, B. Khalili, Novel and convenient one-pot strategy for regioselective synthesis of new 5-aryl-3-methyl-1-phenyl-1,2-dihydro-7a*H*-pyrazolo[3,4-*c*]pyridazin-7a-ol derivatives, Res. Chem. Intermed. 43 (2017) 3925–3937, https://doi.org/10.1007/s11164-016-2848-5;
[a] M. Rimaz, B. Khalili, G. Khatyal, H. Mousavi, F. Aali, A simple and efficient diversity-oriented synthesis of new substituted 3-(arylamino)-6,7-dihydro-1*H*-indazol-4(5*H*)-ones by a KOH-assisted one-pot reaction, Aust. J. Chem. 70 (2017) 1274–1284, https://doi.org/10.1071/CH17146.

[63] M. Rimaz, H. Mousavi, B. Khalili, L. Sarvari, One-pot pseudo three-component condensation reaction of arylglyoxal monohydrates with 1-ethyl-2-thioxodihydropyrimidine-4,6(1*H*,5*H*)-dione for the synthesis of new pyrano[2,3-*d*:6,5-*d'*]dipyrimidines as HIV integrase inhibitor-like frameworks using two different environmentally benign catalytic systems, J. Iran. Chem. Soc. 16 (2019) 1687–1701, https://doi.org/10.1007/s13738-019-01642-1.

[64] M. Rimaz, H. Mousavi, L. Ozzar, B. Khalili, Facile, capable, atom-economical one-pot multicomponent strategy for the direct regioselective synthesis of novel isoxazolo[5,4-*d*]pyrimidines, Res. Chem. Intermed. 45 (2019) 2673–2694, https://doi.org/10.1007/s11164-019-03757-9.

[65] H. Mousavi, A concise and focused overview upon arylglyoxal monohydrates-based one-pot multi-component synthesis of fascinating potentially biologically active pyridazines, J. Mol. Struct. 1251 (2022) 131742, https://doi.org/10.1016/j.molstruc.2021.131742.

[66] M. Rimaz, H. Mousavi, A one-pot strategy for regioselective synthesis of 6-aryl-3-oxo-2,3-dihydropyridazine-4-carbohydrazides, Turk. J. Chem. 37 (2013) 252–261, https://doi.org/10.3906/kim-1210-5.

[67] M. Rimaz, H. Mousavi, B. Khalili, F. Aali, A green and practical one-pot two-step strategy for the synthesis of symmetric 3,6-diarylpyridazines, J. Chin. Chem. Soc. 65 (2018) 1389–1397, https://doi.org/10.1002/jccs.201700470.

[68] F. Sutanto, S. Shaabani, C.G. Neochoritis, T. Zarganes-Tzitzikas, P. Patil, E. Ghonchepour, A. Dömling, Multicomponent reaction–derived covalent inhibitor space, Sci. Adv. 7 (2021) eabd9307, https://doi.org/10.1126/sciadv.abd9307.

[69] D. Zeleke, T. Damena, Advance in green synthesis of pharmacological important heterocycles using multicomponent reactions and magnetic nanocatalysts (MNCs), Results, Chem 7 (2024) 101283, https://doi.org/10.1016/j.rechem.2023.101283.

[70] B. Zeynizadeh, F. Mohammad Aminzadeh, H. Mousavi, Chemoselective reduction of nitroarenes, N-acetylation of arylamines, and one-pot reductive acetylation of nitroarenes using carbon-supported palladium catalytic system in water, Res. Chem. Intermed. 47 (2021) 3289–3312, https://doi.org/10.1007/s11164-021-04469-9.

[71] B. Zeynizadeh, F. Mohammad Aminzadeh, H. Mousavi, Green and convenient protocols for the efficient reduction of nitriles and nitro compounds to corresponding amines with $NaBH_4$ in water catalyzed by magnetically retrievable $CuFe_2O_4$ nanoparticles, Res. Chem. Intermed. 45 (2019) 3329–3357, https://doi.org/10.1007/s11164-019-03794-4.

[72] H. Mousavi, B. Zeynizadeh, R. Younesi, M. Esmati, Simple and practical synthesis of various new nickel boride-based nanocomposites and their applications for the green and expeditious reduction of nitroarenes to arylamines under wet-solvent-free mechanochemical grinding, Aust. J. Chem. 71 (2018) 595–609, https://doi.org/10.1071/CH18200.

[73] C. Sharma, A.K. Srivastava, A. Soni, S. Kumari, R.K. Joshi, CO-free, aqueous mediated, instant and selective reduction of nitrobenzene via robustly stable chalcogen stabilised iron carbonyl clusters ($Fe_3E_2(CO)_9$, E = S, Se, Te), RSC Adv. 10 (2020) 32516–32521, https://doi.org/10.1039/D0RA04491A.

[74] V.S. Sypu, M. Bhaumik, K. Raju, A. Maity, Nickel hydroxide nanoparticles decorated napthalene sulfonic acid-doped polyaniline nanotubes as efficient catalysts for nitroarene reduction, J. Colloid Interface Sci. 581 (2021) 979–989, https://doi.org/10.1016/j.jcis.2020.08.111.

[75] S. Yang, Z.-H. Zhang, Q. Chen, M.-Y. He, L. Wang, Magnetically recyclable metal–organic framework@$Fe_3O_4$ composite-catalyzed facile reduction of nitroarene compounds in aqueous medium, Appl. Organomet. Chem. 32 (2018) e4132, https://doi.org/10.1002/aoc.4132.

[76] M. Pashaei, E. Mehdipour, Silver nanoparticles supported on ionic-tagged magnetic hydroxyapatite as a highly efficient and reusable nanocatalyst for hydrogenation of nitroarenes in water, Appl. Organomet. Chem. 32 (2018) e4226, https://doi.org/10.1002/aoc.4226.

[77] M. Piri, M.M. Heravi, A. Elhampour, F. Nemati, Silver nanoparticles supported on P, Se-codoped g-$C_3N_4$ nanosheet as a novel heterogeneous catalyst for reduction of nitroaromatics to their corresponding amines, J. Mol. Struct. 1242 (2021) 130646, https://doi.org/10.1016/j.molstruc.2021.130646.

[78] Z. Moradi, A. Ghorbani-Choghamarani, $Fe_3O_4$@$SiO_2$@KIT-6@2-ATP@$Cu^I$ as a catalyst for hydration of benzonitriles and reduction of nitroarenes, Sci. Rep. 13 (2023) 7645, https://doi.org/10.1038/s41598-023-34409-z.

[79] P. Mohammadi, M.M. Heravi, L. Mohammadi, A. Saljooqi, Preparation of magnetic biochar functionalized by polyvinyl imidazole and palladium nanoparticles for the catalysis of nitroarenes hydrogenation and Sonogashira reaction, Sci. Rep. 13 (2023) 17375, https://doi.org/10.1038/s41598-023-44292-3.

[80] B. Zeynizadeh, Z. Shokri, M. Hasanpour Galehban, The immobilized Ni(II)-thiourea complex on silica-layered copper ferrite: a novel and reusable nanocatalyst for one-pot reductive-acetylation of nitroarenes, Appl. Organomet. Chem. 33 (2019) e4771, https://doi.org/10.1002/aoc.4771.

[81] M. Esmaeilzadeh, S. Sadjadi, Z. Salehi, Pd immobilized on hybrid of magnetic graphene quantum dots and cyclodextrin decorated chitosan: an efficient hydrogenation catalyst, Int. J. Biol. Macromol. 150 (2020) 441–448, https://doi.org/10.1016/j.ijbiomac.2020.02.094.

[82] J. Kaushik, C. Sharma, N.K. Lamba, P. Sharma, G.S. Das, K.M. Tripathi, R.K. Joshi, S.K. Sonkar, 3D porous $MoS_2$-decorated reduced graphene oxide aerogel as a heterogeneous catalyst for reductive transformation reactions, Langmuir 39 (2023) 12865–12877, https://doi.org/10.1021/acs.langmuir.3c01785.

[83] D. Sharma, P. Choudhary, S. Kumar, V. Krishnam, Interfacial nanoarchitectonics of nickel phosphide supported on activated carbon for transfer hydrogenation of nitroarenes under mild conditions, J. Colloid Interface Sci. 657 (2024) 449–462, https://doi.org/10.1016/j.jcis.2023.11.164.

[84] B. Zeynizadeh, F. Mohammad Aminzadeh, H. Mousavi, Two different facile and efficient approaches for the synthesis of various *N*-arylacetamides via *N*-acetylation of arylamines and straightforward one-pot reductive acetylation of nitroarenes promoted by recyclable $CuFe_2O_4$ nanoparticles in water, Green Process. Synth. 8 (2019) 742–755, https://doi.org/10.1515/gps-2019-0044.

[85] B. Zeynizadeh, R. Younesi, H. Mousavi, $Ni_2B$@$Cu_2O$ and $Ni_2B$@$CuCl_2$: two new simple and efficient nanocatalysts for the green one-pot reductive acetylation of nitroarenes and direct *N*-acetylation of arylamines using solvent-free mechanochemical grinding, Res. Chem. Intermed. 44 (2018) 7331–7352, https://doi.org/10.1007/s11164-018-3559-x.

[86] V. Bilakanti, N. Gutta, V.K. Velisoju, M. Dumpalapally, S. Inkollu, N. Nama, V. Akula, Understanding the role of surface Lewis acid sites of Sn modified Pd/$Al_2O_3$ catalyst in the chemoselective reductive *N*-acetylation of nitrobenzene, React. Kinet. Mech. Catal. 130 (2020) 347–362, https://doi.org/10.1007/s11144-020-01765-0.